Homogenous Sample of Dwarf and Spiral Galaxies to Test MOdified Newtonian Dynamics (MOND)

By

Toky Herimandimby RANDRIAMAMPANDRY

This thesis is submitted to the University of Cape Town in partial fulfilment of the requirements for the degree of Master of Science as part of the National Astrophysics and Space Science Programme

Supersivor: Prof. Claude Carignan

Department of Astronomy
University of Cape Town

March 2013

Abstract

We present mass models for a homogenous sample of dwarf and spiral galaxies. Galaxies with well constrained distances and high quality rotation curves were selected from the literature and their observed rotation curves were confronted with Milgrom's MOdified Newtonian Dynamics (MOND) formalism and the following three dark matter halo models: the observationally motivated pseudo-isothermal dark matter halo (ISO), the cosmologically motivated Navarro, Frenk and White (NFW) halo and the Einasto halo models.

We performed one and two parameter MOND fits and re-estimated the value of the MOND parameter a_0. An average value of $(1.01 \pm 0.10) \times 10^{-8}$ cm s^{-2} was found which is smaller compared to the standard value of 1.21×10^{-8} cm s^{-2}. MOND fits are good for few bright spiral galaxies but some problems were seen for the remaining galaxies in the sample. We also found a correlation between the MOND parameter a_0 and the central surface brightness and the disk scale length of the galaxies. We found that galaxies with larger disk scale length and higher central surface brightness require higher values and galaxies with smaller disk scale length and lower surface brightness prefer lower fit values for a_0. These result could be interpreted as problematic for MOND as a new law of physics since a_0 is considered as an universal constant and should not depend on some galaxies' parameters. However, the observational and systematic uncertainties has to be taken into account to confirm these findings. More investigations are still required for the rotation curves and the conversion of light to mass through the mass-to-light ratio.

For the mass models with dark matter halos, we found that the Einasto halo model

produces better fits to the rotation curves compared to the other models. This is true for the model with M/L fixed and M/L free. The fits are remarkably good for M/L free, the Einasto halo model with M/L free preferred the disk-less (M/L = 0) model for more than half of the galaxies in the sample which is unphysical. The reduced qui-squared for the Einasto halo with M/L fixed ($< \chi_r^2 > = 1.01$) is smaller compared to the ISO halo ($< \chi_r^2 > = 1.94$), the NFW halo ($< \chi_r^2 > = 2.16$) and MOND with a_0 free ($< \chi_r^2 > = 2.47$) models.

However, the unphysical stellar disks obtained suggest that the goodness of the Einasto halo fits is not sufficient to favour this model over the others. This is why, considering the more realistic stellar disks obtained with the ISO halo models, we can say that they produce the best representation of the observed rotation curves. The dark matter halo scaling laws reported in the literature were found in our data for the ISO dark matter halo. Correlation between the central density ρ_0 and the core radius r_c were found, thus the central halo could be characterised by one parameter since the central density and core radius of the halo are correlated. We also found that low-luminosity galaxies tend to have smaller core radii and higher central densities which is in good agreement with previous studies. We also re-affirm that the dark matter halo surface density is nearly constant. We found $\rho_0 \; R_C \sim 120 M_\odot \; pc^{-2}$ which in good agreement with previous studies.

These results need to be verified with larger samples with well determined rotation curves, well constrained distances and good quality luminosity profiles before final conclusions can be drawn.

Declaration

I, Toky H. Randriammpandry, hereby declare that the work on which this dissertation is based is my original work (except where acknowledgements indicate otherwise) and that neither the whole work nor any part of it has been, is being, or is to be submitted for another degree in this or any other university. I empower the university to reproduce for the purpose of research either the whole or any portion of the contents in any manner whatsoever.

I know the meaning of Plagiarism and declare that all of the work in the document, save for that which is properly acknowledged, is my own.

Signature:

Date: .

Keywords and Abbreviations

Keywords

Cosmology: Dark Matter

Galaxy: dynamics, rotation curves

Galaxies: Mass discrepancies

Abbreviations

MOND: MOdified Newtonian Dynamics

GIPSY: Gronegen Image Processing SYstem

ISM: InterStellar Medium

CDM: Cold Dark Matter

LSB: Low Surface Brightness

HSB: High Surface Brightness

THINGS: The HI Nearby Galaxy Survey

Acknowledgements

I would like to thank my supervisor Prof. Claude Carignan for his tireless effort and guidance during the realisation of this project.

I would like to express my gratitude to Prof. Erwin de Blok and the entire THINGS team for providing us with their data and results.

We would like to thank Dr. Laurent Chemin for helping us with the Einasto halo models and Dr Gentile Gianfranco for sending us his result for MOND with two free parameter fits.

I would like to extend my thanks to the following people with no particular order: Dr Garry Angus, Dr Danielle Lucero, Mr Solohery R., Mrs Nicky Walker (NASSP Administrator), Mrs Carol Marsh (Astronomy Department), Ms Bongiwe Ndamane (NRF/UCT), all my classmates and colleagues, my parents and last but not least to my wife Mrs Manohisoa R.

I acknowledge the department of Astronomy at the University of Cape Town for hosting this research and the South African Square Kilometre Array Project for the funding.

Contents

List of Tables

List of Figures

Chapter 1

Introduction

1.1 Background

Galaxies are known to be the building block of the universe. They are composed of the stars and the interstellar medium (ISM). The interstellar medium (ISM) is composed of gas and dust clouds. However, most of the mass in galaxies resides in the form of unseen matter, the so-called "dark matter". Dark matter is an unknown form of matter that contributes most to the total mass of the galaxies: therefore it plays an important role in its dynamics. Better understanding of the matter distribution of galaxies will enable us to construct more accurate models for the mass content of the universe.

In cosmology, the commonly adopted model is the ΛCDM model which assumes that about twenty five percent (25 %) of the total mass-energy budget of the universe is in the form of Cold Dark Matter (CDM), and seventy percent (70 %) in the form of dark energy, which is represented by the cosmological constant Λ. The ordinary matter or baryonic matter only contributes less than five percent (5 %) of the total mass of the universe. It has been shown that the ΛCDM models can reproduce the structure formation history of the universe and the primordial density fluctuation spectrum during the period of inflation but fails to explain the dynamics

and kinematic of dwarf and spiral galaxies. Therefore, studies of the dynamics of spiral and dwarf galaxies will give us a hint as to whether the current model is correct or if an alternative model is needed to explain the different aspects of the observations.

1.1.1 Galaxy Classification Schemes

It is necessary to classify galaxies in order to study their evolution and their mass content. This also enable us to identify them and provide more insight of their physical properties. Galaxies are classified based on their morphology, their stellar and gas content as well as their rotational velocity. There are several classification schemes in the literature, but the two well know classification schemes are: the Hubble classification scheme or Hubble sequence and the de Vaucouleurs classification scheme.

Hubble Slassification Scheme

The Hubble classification scheme was developed by Edwin Hubble in 1926 (Hubble 1926) to classify galaxies depending on their morphological appearance. Hubble used photographic (optical) images and classifies galaxies into 3 classes

- Elliptical galaxies
- Spiral galaxies
- Irregular galaxies

Lenticular galaxies were added to the scheme for continuity. Hubble believed that there must be a morphological transition between Ellipticals and Spirals which are lenticulars. Lenticular galaxies have a prominent bulge and disk-like structure.

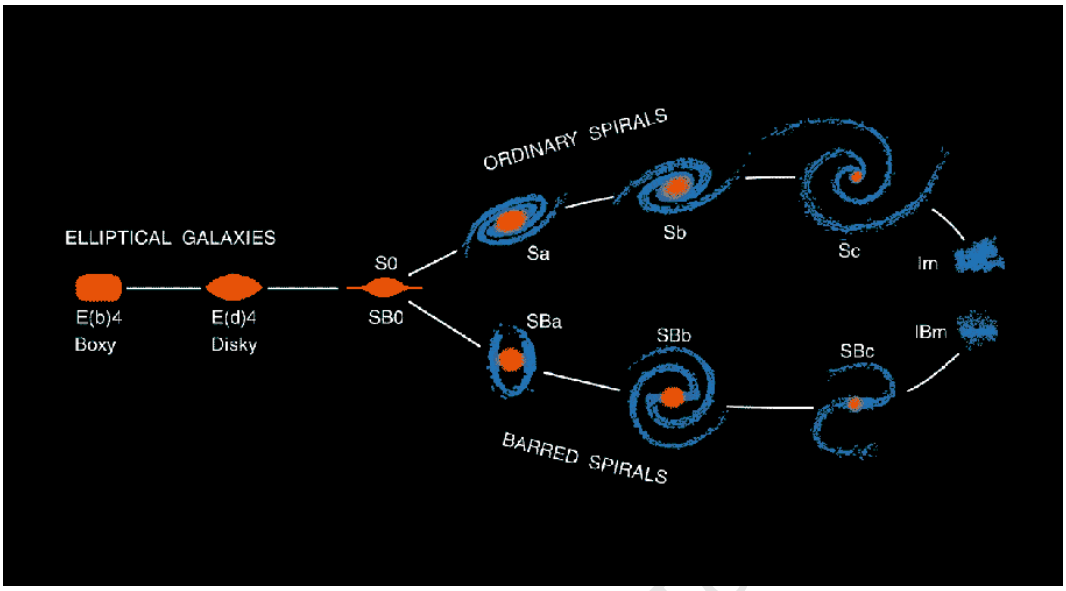

Figure 1: Hubble classification scheme: The Hubble tuning fork diagram

Hubble classification criteria were: the size of the central bulge, the degree of resolution in the arms and the openness of the spiral arms. The Hubble tuning fork diagram shows a schematic views of the Hubble sequence, it is shown in figure 1. Elliptical galaxies are located at the left end in the diagram, followed by lenticulars, spirals and irregular galaxies. Brief descriptions on each class are given below:

1. Elliptical galaxies have an elliptical shape and are populated by old population II stars with very little gas. Elliptical galaxies are mostly located in clusters and groups. They are very massive objects and non-rotating or slow-rotating. For example, a giant elliptical is twice as big as the Milky Way galaxy in size. Elliptical galaxies are also subdivided into subclasses depending on their ellipticity, which is the ratio between the major and minor axis.

2. Lenticular galaxies consist of a central bulge surrounded by a flat disk. The disk has no spiral arm structure and mostly occupied by dust, which make the disk less visible in optical compared to the central bulge. Most of the observed light in the optical are emitted from the central bulge populated by

old bright population II stars. Lenticular galaxies are the intermediate class between elliptical and spiral galaxies. Some lenticular galaxies also have bars, therefore they are classified as SO for unbarred lenticular and SBO for barred lenticular. Lenticular and spiral galaxies are also known as disk galaxies.

3. Spiral galaxies are composed of a central bulge and a disk with spiral arm structure. The bulge components are populated by old stellar populations (population II stars) and the spiral arms by young populations I stars. The flat rotating disk is composed by young and old population I stars, neutral gas, HII regions and dust. Furthermore, the dust and gas are squeezed by density waves and form the spiral arm structures. The young stellar population (O & B stars) in the arms is very luminous which makes the spiral arms look brighter compared to the rest of the galaxy in the optical. Spiral galaxies are supported by rotation such that their rotation speed can be used as a tracer of the mass distribution within the galaxy.

4. Irregular galaxies have no particular shape and cannot be classified as spiral galaxies. They are small in size and less luminous. The gas and stellar contents of irregular galaxies are spread randomly. Their large gas content makes them perfect objects to study the distribution of dark matter.

Hubble also sub-divided ellipticals and spirals into sub-classes:
Elliptical galaxies were sub-classified depending on the the shape of the ellipse. The sub-class is denoted by a number (En) where n goes from 0 to 7. Elliptical galaxies with rounded shape are classify as E0 and those with elongated shape as E7. The number which determines the subclass is obtained using the following formula:

$$\epsilon = 10(1 - a/b) \tag{1}$$

Where a is the semi-major axis of the ellipse and b the semi-minor axis. Spiral galaxies are sub-classified as function of the openness of the spiral arms and their stellar content. Spiral galaxies are sub-classified as Sa,Sb and Sc. Sc spiral galaxies have open spiral arm structures.

The de Vaucouleurs Classification Scheme

Prompted by the work of Hubble on classifying nebulaes, a revised version of the Hubble classification was published by Sandage (1961) in his book "Hubble Atlas of Galaxies". Spiral and Lenticular galaxies are sub-divided into barred and unbarred depending on the presence of bar structure. Alternative classes were also introduced, for example a spiral galaxy with a strong bar structure is denoted by SB and with a weak bar structure with SAB.
The most significant modification of the Hubble classification which is now widely used was introduced by Gérard de Vaucouleurs in 1956 by developing the classification *volume* (de Vaucouleurs 1956). The de Vaucouleurs classification scheme classifies galaxies in three dimensions as shown in figure 2:

- the first and horizontal dimension represent the continuity of morphological forms ranging from Elliptical galaxies to Irregular galaxies;
- the second and vertical dimension differentiate between galaxies with bars and without bars;
- the third dimension distinguishes galaxies with pure ring system (r) and spiral arm subtypes (s).

The classification volome by de Vaucouleurs (1956) is presented in figure 2, which was reproduced by Ron Buta with more details.

Morphological Types and Galaxy Evolution

The Hubble sequence was believed to be an evolutionary track so that late type galaxies become early type galaxies once their gas content are used up and transformed into stars. The validity of this hypothesis is still a matter of debate. For example, the presence of bars structure could change the morphology of galaxies. The presence of bar can drive spiral arm density waves or generate resonance rings

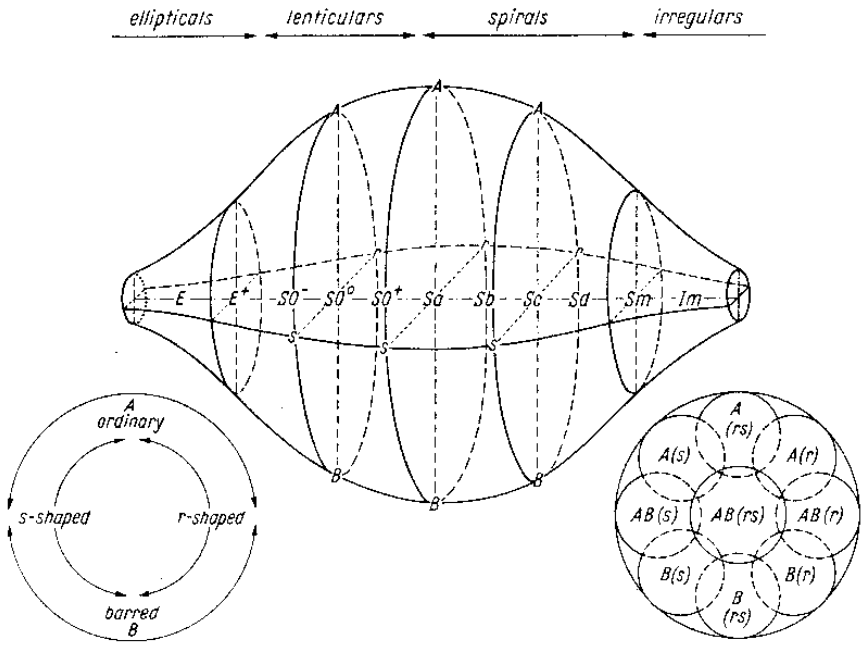

Figure 2: Schematic representation of the de Vaucouleurs classification scheme: an extension of the Hubble sequence (image courtesy of Ron Buta)

of gas (Kormendy & Norman 1979).

From hydrodynamic simulation, Bournaud & Combes (2004) found that bars are transient features with a lifetime of 1 to 4 Gyrs. Therefore, galaxies could transform from barred to unbarred or vice versa due to this bar dissolution and reformation mechanism. The phenomena of galaxy interaction, secular evolution and gas accretion are also very important mechanisms in galaxy evolution and morphological classification studies.

1.1.2 Rotation Curves of Galaxies

Velocity Fields

The rotation curves of galaxies are derived from the rotational velocities of stars and gas at different radius. In practice, galaxy rotation curves are derived from the velocity field of the stars or of the ionized gas in the optical and of the neutral

hydrogen (HI) or the molecular gas in radio. The velocity field is the distribution of the rotation velocity of the galaxy calculated from the doppler shift of the Hα line emission in the optical and of the HI line emission in radio. The velocity field map shows the direction and magnitude of the rotational velocity of the gas and stars.

In the optical, emission lines from optical spectra such as Hα lines of the ionized gas are used to derive the velocity field and stellar absorption lines for the stars mainly in the centre of the galaxy Optical rotation curves provide more details on the dynamics of the inner part of the galaxies due to higher spatial resolution. On the other hand, rotation curves derived from the 21 cm lines are more extended, up to 5-10 disk scale lengths. The 21 cm observation is known to be the most powerful tools to study the distribution of mass in galaxies because it probes the gravitational potential further out. The 21 cm line is due to the spin flip of a neutral hydrogen atom, a photon is emitted and it is observed in the radio part of the electromagnetic spectrum precisely at 1.4 GHz. The observations are obtained with a single dish or an aperture synthesis array. Rotation curves are derived by applying a tilted-ring model to the velocity field. The 21 cm lines have a radial extent greater than the visible disk, which allow us to study the kinematics of the outer parts of the galaxy. This line also provides information on the distribution of the neutral hydrogen gas.

Tilted Ring Models

A set of concentric rings is used to describe the motion of the gas in a galaxy. The gas is assumed to be in a circular motion. Each rings is characterized by an inclination, a Position Angle P.A., systemic velocity V_{sys} and rotation velocity V_C. The line of sight velocity at any (x,y) position on a ring with radius R is given by

$$V(x,y) = V_{sys} + V_C sin(i) cos(\theta) + V_{exp} sin(i) cos(\theta) \quad (2)$$

where θ is the position angle with respect to the receding major axis measured in the plane of the galaxy, V_{exp} is the expansion velocity. V_{exp} is usually set to be zero except for systems such as starburst galaxies.

θ is related to actual P.A. in the plane of the sky by the following formula.

$$cos(\theta) = \frac{-(x - x_0)sin(P.A.) + (y - y_0)cos(P.A.)}{R} \quad (3)$$

$$sin(\theta) = \frac{-(x - x_0)cos(P.A.) + (y - y_0)cos(P.A.)}{Rcos(i)} \quad (4)$$

The tilted ring model has been fully implemented in the GIPSY task ROTCUR (Begeman 1989).

de Blok et al. (2008) used the GIPSY task ROTCUR to derive the rotation curves of 19 nearby galaxies drawn from THINGS. They used a $|cos\theta|$ wieghting for all the fits. The width and radii of the tilted rings were defined with a rate of two data points per synthesized beam width. The rotation curves were derived using the following procedures:

Firstly, the position of the center for each galaxy was fixed using the values found by Trachternach et al. (2008). Secondly, the task ROTCUR was run twice in order to estimate V_{sys}, i and P.A. ROTCUR uses a non-linear least square fit to determine these parameters with initial values for each parameter which could be determined using optical images. And finally, the i and P.A. were fixed and the rotation curves were derived.

The uncertainties on the rotation curves were estimated using the dispersion of the velocity values along the tilted ring which is more physical compared to the 1 σ error. Another source of uncertainties is the difference between receding and approaching side, this was quoted as pseudo-1σ uncertainties. Thus, the dispersion found along the rings and the pseudo-1σ form the uncertainties in the rotation curves.

1.2 Mass Discrepancies in Galaxies

It is well known that there is a need for more mass than that from the stars, dust and gas alone. By measuring the velocity dispersion of the galaxies in the coma cluster F. Zwicky (1933) found that the velocity dispersion of the galaxies was too

high which requires more mass than the sum of the individual galaxies to keep the galaxies gravitationally bound. A schematic view of the mass discrepancy is shown in figure 3. The bold green line is obtained using Newtonian dynamic without dark matter and the obverved rotation curves taken from de Blok et al. (2008) are shown as points.

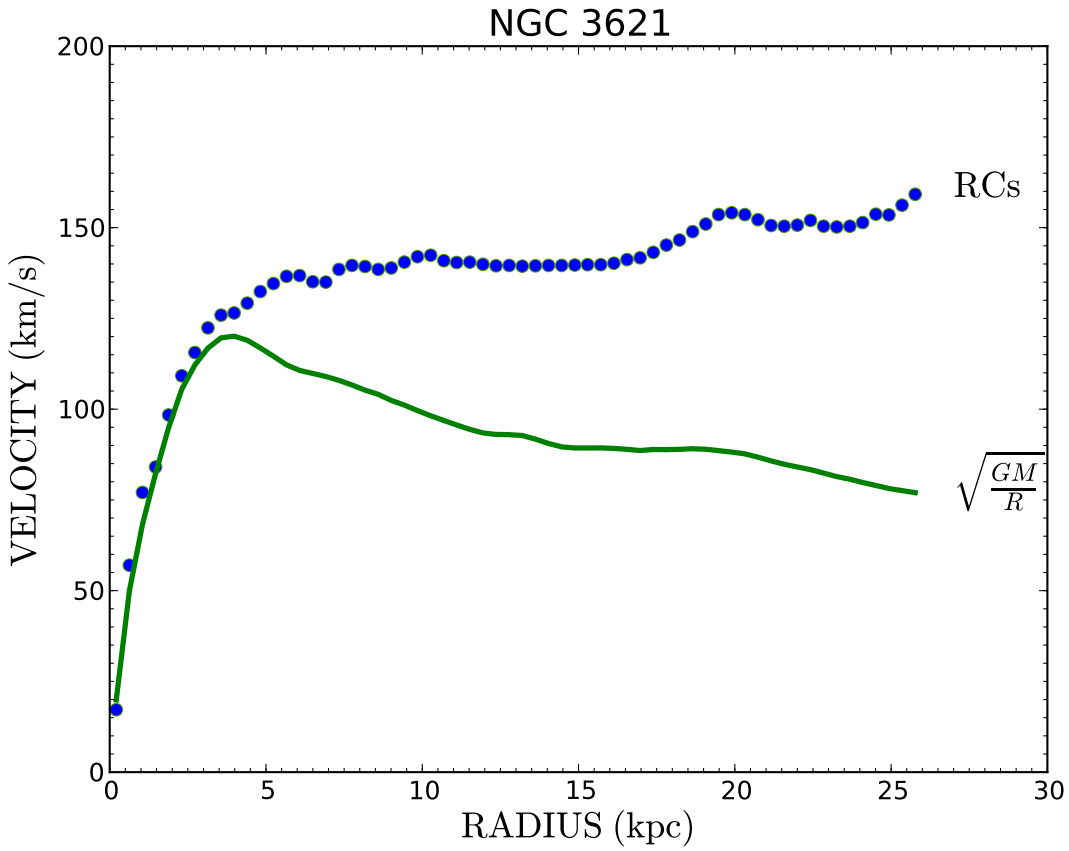

Figure 3: Observed rotation curves of NGC 3621 compared with Newtonian rotation curve calculated from the observed mass distribution of the stars and the gas.

The flatness of the rotation velocity at large radius implies that there might be more mass in the outer parts of the galaxies to keep the velocity constant. Early observations of HI rotation curves have shown that most spiral galaxies have flat rotation curves (e.g. Shostak 1973; Roberts & Whitehurst 1975; Bosma 1978). This flatness of rotation curves of spiral galaxies indicates a large mass discrepancies in these objects. The rotational velocity of a rotating object such as a galaxy is expected to decrease toward the edge in the Newtonian dynamic framework. However, the rotation curves stay flat far beyond the optical radius (see: Bosma 1978; de Blok et al. 2008).

For a model with a dark matter halo, the commonly accepted hypothesis is to assume a more or less spherical halo of unseen dark matter in addition to the visible mass. The distribution of dark matter in galaxies is defined by a theoretical or empirical density distribution profile. Several density profile models of the distribution of dark matter are presented in the literature.
The three model most frequently used are:

- The pseudo-isothermal halo dark matter model (ISO) (observationally motivated model)
- Navarro-Frenk-White (NFW) dark matter halo model (Navarro et al. 1997) (derived from N-body simulations)
- Einasto dark matter halo model (Einasto 1969)

Another model to explain the missing mass problem is the MOdified Newtonian Dynamics (MOND). MOND was proposed by Milgrom (1983b) as an alternative to dark matter. Milgrom postulated that at small acceleration the usual newtonian dynamics breaks down and the law of gravity need to be modified. A theory like MOND should have the ability to explain the different aspect of observations and has familiar physical roots. MOND has been claimed to be able to explain the mass discrepancies in galaxies without dark matter with an additional constant a_0 (Milgrom 1983a) which has a dimension of acceleration.

1.3 Solution to the Mass Discrepancies: Dark Matter Halo

As mentioned previously, most of the mass in galaxies is in the form of unseen matter called "Dark matter". Dark Matter is an unknown form of matter which does not interact with ordinary matter, it is undetected and its existence is only known from its gravitational effect on luminous matter (the bending of light for the galaxy clusters and the flatness of galaxy rotation curves). The common scenario is that galaxies are embedded in dark matter halos, which follow theoretical density distribution profiles. Here we describe the three well known density distribution profiles (more explanations are given in Chapter 3 section 3): the pseudo-isothermal (ISO) dark matter halo with a constant density core, the Narravo, Frenk and White (NFW) halo with a cusp central density and the Einasto halo model.

1. The pseudo-isothermal dark matter halo profile is an observationally motivated model dominated by a constant central density core.

$$\rho_{ISO} = \rho_0[1 + (\frac{r}{r_c})^2]^{-1} \tag{5}$$

The density profile is given by equation 1 where ρ_0 is the central density and r_c the core radius.

2. The Navarro, Frenk and White dark matter halo model (NFW) is derived from cosmological simulations. NFW models are in good agreement with the ΛCDM model and therefore commonly accepted in cosmology. It has a cusp central density core (Navarro et al. 1997). The density profile of NFW model is given as:

$$\rho_{NFW} = \frac{\rho_i}{\frac{r}{r_s}(1 + \frac{r}{r_s})^2} \tag{6}$$

where ρ_i is the density of the universe when the dark matter collapse and r_c a scale radius.

3. It has been debated that the NFW could not explain the observed rotation curves of spiral and dwarf galaxies as compared to the observationally motivated ISO model. High resolution N-body simulations predicted central cusp core for the central halo. However most of the available data from observations support the constant central density core rather than the cusp core predicted by the NFW model. This is known as the cusp-core problem. Therefore, Navarro et al. (2004) introduced a new model similar to the Sérsic function for the distribution of light in elliptical galaxies. Later, it was found that Einasto was the first who used this model for the distribution of mass in galaxies (Einasto 1969). The density profile of the Einasto dark matter halo model is given by

$$\rho_E = \rho_{-2} exp(-2n[(\frac{r}{r_{-2}})^{\frac{1}{n}} - 1]) \quad (7)$$

where, r_{-2} is the radius where the density profile has a (logarithm) slope of -2 , ρ_{-2} is the local density at that radius and n is the Einasto index .

1.4 Alternative to Dark Matter: Modified Newtonian Dynamics (MOND)

1.4.1 The Basis

The total gravitational forces for any rotating object is obtained by using the virial theorem relation. The virial theorem is valid under the following assumptions:

- Gravity is the only force which governs the dynamics of the system
- The gravitational force depends only on the mass and the distribution of the mass of the particle in a conventional way
- Newtons second law holds

However, these assumptions are not satisfied for galaxies and galaxy systems which exhibit small accelerations (Milgrom 1983b) because the inertia force is not the same as the gravitational force. Milgrom postulated that if the conventional newtonian dynamics is modified at small acceleration then the above assumptions will be satisfied and the mass discrepancies in galaxies will also disappear. The MOND theory postulates that at a small acceleration the newtonian dynamics break down and MOND should be applied. The transition between the newtonian and MONDian regime is characterised by an acceleration threshold value called a_0 below which MOND should be used. In the MOND framework, the gravitational acceleration of a test particle is given by :

$$\mu(x = g/a_0)g = g_N \tag{8}$$

where g is the gravitational acceleration, μ(x) is the MOND interpolating function and g_N the newtonian acceleration. The interpolating function defines the transition between Newtonian and low acceleration regime. The interpolating function is explained in detail in section 1.4.3.

1.4.2 MOND Acceleration Constant a_0

In the context of MOND, Milgrom (1983b) introduced a new universal constant a_0 with a dimension of acceleration. As an universal constant, a_0 should be the same for all astrophysical objects. However, the observational uncertainties could introduce large scatter on a_0 and have to be taken into account. Significant departures on a_0 from the standard value could be interpreted as being problematic for MOND. The implication of this new constant in cosmology is now also a matter of debate. A correlation between a_0 and the cosmological constant and the Hubble constant have been presented in the literature. A complete review about the implications of MOND in cosmology can be seen in Famaey & McGaugh (2012). Milgrom estimated a_0 parameter using Freeman's law which stipulates that disk galaxies have typical extrapolated central surface brightness in the B band (Freeman 1970) of 21.65 mag

arcsec^{-2} . Milgrom estimated a_0 to be $\sim (0.7-3)\times 10^{-8}(M/L)_*\ cm\ s^{-2}$. There are other methods that could be used to find a_0, such as the Tully-Fisher relation. The preferred method to estimate a_0 is by comparing the calculated rotation curves from the observed mass distribution and the observed rotation curves and take a_0 as a free parameter.

1.4.3 MOND Interpolating Functions

The shape of the rotation curves is predicted by the MOND interpolating function. This function is not clearly defined but its characteristic is specified (Milgrom 1983). The interpolation function or μ-function should have the following asymptotic behaviours.

$$\mu(x) = 1\ if\ x \ll 1$$

$$\mu(x) = x\ if\ x \gg 1$$

where x is the ratio between the gravitational acceleration and the MOND acceleration constant a_0.

The general form introduced for the interpolating function is:

$$\mu_n(x) = \frac{x}{(1+x^n)^{1/n}} \tag{9}$$

The simple μ-function corresponds to n = 1 :

$$\mu(x) = \frac{x}{1+x} \tag{10}$$

And the standard μ-function corresponds to n = 2:

$$\mu(x) = \frac{x}{\sqrt{1+x^2}} \tag{11}$$

Famaey & Binney (2005) found that the simple interpolating function gives plausible M/L compared to the standard μ-function.

The interpolating function with n larger than 2 could be used for solar system objects.

Other example of μ-function are presented in the literature:

$$\mu(x) = 1 - e^{-x} \ (Expo) \tag{12}$$

$$\mu(x) = 1 - (1 + x/3)^{-3} \ (Polyn) \tag{13}$$

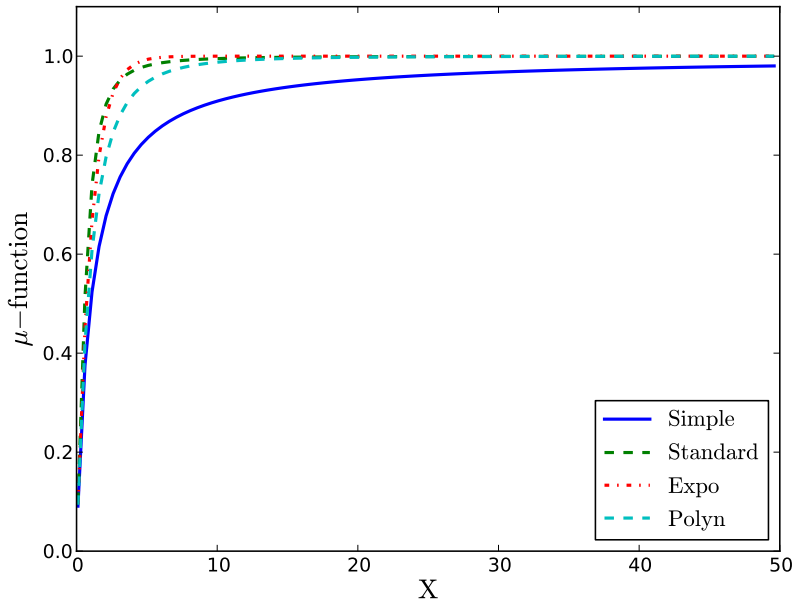

Figure 4: Different forms of the interpolating functions from the literature, lines are described on the graph.

Different forms of the interpolating functions are shown in Figure 4. The main difference between these functions are the transition from the newtonian to the MONDian regime. The standard and exponential μ-function are steeper compare to the simple μ-function. All these functions have the asymptotic behaviour which means that at large value of x, the μ-function becomes asymptotically flat. More explanations on how the MOND rotation curves was derived are given in Chapter 3 section 4.

1.5 Previous Work

MOND is an alternative explanation of the mass discrepancies in galaxies without dark matter. The phenomenological success of MOND to reproduce the observed rotation of galaxies has attracted a huge interest in the astronomy community for the last three decades. One of the first studies was made by Kent (1987) using HI rotation curves of spiral galaxies and his conclusion was not in favour of MOND. Kent's work was criticised by Milgrom (1988) who pointed out errors in distances and inclinations, which needed to be corrected. Dwarf galaxies are critical to test a theory such as MOND because these objects present the largest discrepancies between the visible mass and the dynamic mass. Lake (1989) concluded that MOND could not predict the observed rotation curves of a sample of dwarf galaxies where luminous mass is dominated by gas and not stars. However, Milgrom (1991) once again disapproved Lake's conclusion by mentioning the large errors in the distances and inclinations which need to be taken into account.

Begeman et al. (1991) was the first to estimate the value of a_0 by fitting the rotation curves of four bright spiral galaxies. The calculated rotation curves derived from the observed mass distribution were compared to the observed rotation curves. The MOND parameter a_0 was taken as a free parameter during the fitting procedure. Begeman et al. (1991) found an average value of $a_0 = 1.21 \times 10^{-8}$ cm s^{-2}. This result was confirmed by Sanders (1996) and Sanders & Verheijen (1998) using the same method. This is now assumed as the standard value for a_0 . However, Bottema et al. (2002) found that a lower value for a_0 (0.9×10^{-8} cm s^{-2}) yielded better fits to the rotation curves.

A complete review about the previous tests of MOND is presented in Sanders & McGaugh (2002). In that review the basic framework of MOND is explained. Rotation curves fits using MOND prior to 2002 are presented and the different capabilities of MOND are listed. The most recent review on MOND and its implications to cosmology was done by Famaey & McGaugh (2012).

The analysis by de Blok & McGaugh (1998) was the first to use LSB galaxies in the context of MOND. LSB galaxies are good candidates to test MOND because their acceleration fall below the MOND acceleration limit a_0. de Blok & McGaugh (1998) used a sample of 15 LSB galaxies and modelled their mass distribution using the MOND formalism . They found that MOND is successful in reproducing the shape of the observed rotation curves for three quarter of the galaxies in the sample. The most recent study of LSB galaxies in the context of MOND was done by Swaters et al. (2010). MOND produced acceptable fits for also three quarter of the galaxies in their sample. The correlation between a_0 and the extrapolated central surface brightness of the stellar disk was also investigated. Swaters et al. (2010) found that there might be a weak correlation between a_0 and the R-band surface brightness of the disk. This is shown in their Figure 7. Their interpretation was that galaxies with lower central surface brightness had lower values for a_0 and galaxies with higher central surface brightness had higher values for a_0. Such a correlation would be in contradiction with MOND as an universal laws and a_0 as an universal constant. The reliability of the mass models with MOND depends strongly on the sensitivity and spatial resolution of the observed rotation curves. More extended rotation curves are needed to trace the matter up to the edge of the galaxies but higher resolution is required in the inner parts. Rotation curves derived from The HI Nearby Galaxy Survey or THINGS (Walter et al. 2008) sample satisfy these criteria. THINGS consists of 34 dwarfs and spiral galaxies observed with the Very Large Array in the B, C and D configurations at the 21 cm wavelength. The rotation curves of 19 galaxies from THINGS derived by de Blok et al. (2008) are the highest quality rotation curves available in the literature. Gentile et al. (2011) used a subsample of 12 galaxies from de Blok et al. (2008) and modeled their mass distributions using the MOND formalism. They performed one and two parameters MOND fits and recalculated the value of a_0 and found a similar value to the standard one which was estimated by Begeman et al. (1991).

Their average value is $a_0 = 1.22 \times 10^{-8}$ cm s^{-2} using the simple μ-function. They also looked at the correlation between a_0 and central surface brightness in the 3.6 micron bands and found that there was no correlation. However their points have a large scatter. Moreover, the bulge central surface brightness were used instead of the extrapolated disk central surface brightness.

1.6 Outline of the Thesis

A sample of fifteen (15) dwarf and spiral galaxies were selected from the literature. These galaxies were selected to be homogenous in terms of their measured distances, the sampling of their rotation curves and they span a wide range of luminosities and morphological types. The rotation curves will be confronted with the MOND formalism and dark matter halo models. The aim is to test the validity of MOND as a new law of physics and also to confirm the existence of the dark matter scaling laws.

This work is organised as follow: Chapter 1 is the introduction, the sample selection is presented in chapter 2, the methods for the mass models are explained in chapter 3, results and discussions are shown in chapter 4 and finally, conclusions and future work are presented in chapter 5.

Chapter 2

Sample Selection

2.1 The Sample

This work aims to select a sample of dwarf and spiral galaxies with accurately measured distances and high quality rotation curves and to model their mass distributions using the MOND formalism and dark matter halo models. Therefore, the selection criteria for the sample are based on the method used to determine the distance, the morphological type and the availability of high quality HI rotation curves in terms of spatial resolution and sensitivity.
The selection criteria are therefore:

1. Cepheid based distances are commonly adopted to be the most accurate to measure distances of nearby galaxies. The relationship between the brightness and the period of variability of the cepheid variables is used to determine the distance. The distance of the galaxy is then obtained by averaging the distances of all the cepheids. The method used to measure the distance and references from where the distances where collected are shown on column 5 of table 1.

2. The second criteria is to have a sample of galaxies spanning a wide range of luminosities and morphological types from dwarf irregular to bright spiral

galaxies. Therefore DDO 154 and IC 2574 are included even if cepheid distances are not available. Furthermore, these two galaxies are gas dominated galaxies and exhibit large discrepancies between their visible mass and the dynamical mass which makes them ideal object to test MOND and dark matter halo models.

3. The last criteria is the availability of HI rotation curves having a larger radial extend compared to optical rotation curves

The final sample includes fifteen (15) dwarf and spiral galaxies. Eleven galaxies are part of THINGS, where their rotation curves were derived by de Blok et al. (2008). These rotation curves were derived with two data points per resolution element. Resampled version of the rotation curves with only one point per beam will be used in this study such that every points are independent, which is necessary for the chi-squared analysis (cf. section 3.4 for more explanation). The rotation curve and gas distribution of NGC 3109 are taken from Jobin & Carignan (1990) and from Westmeier et al. (2011) for NGC 300. NGC 55 and NGC 247 are both members of the Sculptor group of galaxies. The rotation curve of NGC 55 was taken from Puche & Carignan (1991) and from Carignan & Puche (1990) for NGC 247.

Properties of the galaxies in the sample are shown in table 1. The column are described as follows: column 1: galaxy name, column 2 and 3 Position Angle and Inclination taken from de Blok et al. (2008) except for NGC 3109, NGC 300, NGC 55 and NGC 247. For these four galaxies their Position Angles and Inclinations were collected from the same sources as their rotation curves. These parameters were derived using the tilted ring method as described in de Blok et al. (2008). Column 4 is the distance with the estimated errors taken from the original paper. Seven galaxies in this sample are part of Hubble Space Telescope key project which aimed to measure the Hubble constant (Kelson et al. 2000). The final results of the cepheid distances from this project are summarised in Freedman et al. (2001). The distance of DDO 154 and IC 2574 were taken from Karachentsev et al. (2004) which use the brightest blue stars for DDO 154 and the tip of red giant branch for IC 2574. The

Table 1: Properties of the galaxies in the sample

Name	P. A.	Incl.	Distance	Method[Ref]	m_B	M_B	Type
	°	°	Mpc		mag	mag	
1	2	3	4	5	6	7	8
DDO 154	230	66	4.30 ± 0.54	bs[K04]	13.94	-14.23	IB(s)m
IC 2574	53.4	55.7	4.02 ± 0.41	rgb[K04]	10.80	-17.21	SAB(s)m
NGC 0055	109.7	76.9	1.94 ± 0.03	cep[G08]	9.60	-16.79	SB(s)m
NGC 0247	170.0	74.0	3.41 ± 0.17	cep[G09]	9.70	-17.95	SB(s)cd
NGC 0300	310.5	42.3	1.99 ± 0.04	cep[G05]	8.72	-17.67	SA(s)d
NGC 0925	286.6	66.0	9.16 ± 0.63	cep[F01]	10.69	-19.13	SAB(s)d
NGC 2366	39.8	63.8	3.44 ± 0.31	cep[T95]	11.53	-16.13	IB(s)m
NGC 2403	123.7	62.9	3.22 ± 0.14	cep[F01]	8.93	-18.60	SAB(s)cd
NGC 2841	152.6	73.7	14.10 ± 1.50	cep[F01]	10.09	-20.66	SA(r)b
NGC 3031	330.2	59.0	3.63 ± 0.25	cep[F01]	7.89	-19.89	SA(s)ab
NGC 3109	93.0	75.0	1.30 ± 0.02	cep[S06]	10.39	-15.18	SB(s)m
NGC 3198	215.0	71.5	13.80 ± 0.95	cep[F01]	10.87	-19.83	SB(rs)d
NGC 3621	345.4	64.7	6.64 ± 0.46	cep[F01]	10.28	-18.82	SA(s)d
NGC 7331	167.7	75.8	14.72 ± 1.02	cep[F01]	10.35	-20.49	SA(s)b
NGC 7793	290	50	3.43 ± 0.10	cep[P10]	9.17	-18.79	SA(s)d

F01: Freedman et al. (2001); S06: Soszyński et al. (2006); K04: Karachentsev et al. (2004); T95: Tolstoy et al. (1995); P10: Pietrzyński et al. (2010); G05: Gieren et al. (2005); G08: Gieren et al. (2008); G09: Gieren et al. (2009)
col. 1: Galaxy name; col. 2: Position Angle; col. 3: Inclination; col. 4: Distance with the uncertainty; col. 5: Method used to measure the distance & reference; col. 6: apparent magnitude taken from the RC3 catalog; col. 7: Absolute magnitude; col 8: Morphology type.

column 5 is the method used to estimate the distance and reference, column 6 and 7 are the apparent and absolute magnitudes respectively. The apparent magnitudes were taken from the RC3 catalogue (de Vaucouleurs et al. 1991) and converted into absolute magnitude via the distance modulus formulas. The last column is morphological types.

2.2 Descriptions of the Individual Galaxies

2.2.1 THINGS Galaxies

The HI Nearby Galaxy Survey or THINGS (Walter et al. 2008) is a large HI observing program of 34 dwarf and spiral galaxies covering a wide range of physical properties. Most of the galaxies in the THINGS sample were drawn from SINGS (Kennicutt et al. 2003). SINGS was designed to study the small structure of the ISM at different wavelength bands. There are few galaxies in THINGS which are not part of the SINGS sample because some of the objectives of THINGS are not covered by SINGS due to time constraint on the Spitzer space telescope. Thus, SINGS does not include small dwarfs galaxies in their sample.
The main objectives of THINGS are;

- study of the atomic gas and of the small-scale structure of the ISM
- deeper analysis of the rising part of the rotation curves and their shape
- study of the star formation history

In order to achieve these goals, high sensitivity and high spatial and velocity resolutions were needed. The observation were done with the Very Large Array of the National Radio Astronomy Observatory in the B, C and D configurations. The B configuration provides high spatial resolution but is only sensitive to small-scale therefore the C and D configurations data are needed for the large scales. One of

the main goal of THINGS was to reach a spatial resolution less than 500 pc, this requires an angular resolution of about 6 arcsecs for a distance < 15 Mpc. THINGS also has a spectral velocity less than 5.2 km s^{-1} and a sensitivity of 0.4 mjy $beam^{-1}$ which correspond to a column density of about 3.2×10^{20} cm^{-2} using B configuration of the VLA. Because of its sensitivity, high spatial and velocity resolution, the THINGS data are the highest quality HI data available to date.

The data were reduced using standard routines implemented on the AIPS software. The VLA standard calibrators 3C286 = J1331+305 and 3C48 = J0137+331 or 3C147 = J0542+498 were used as primary and secondary calibrators (cf Walter et al. 2008 for more detail on the data reduction). THINGS data products are made available publicly. The data products consist of data cubes, HI maps and velocity maps. The rotation curves of 19 galaxies drawn from THINGS were derived by de Blok et al. (2008) using tilted ring model (cf. section 1.3). In this project, eleven galaxies are part of the THINGS sample. More details on the individual galaxies are given below.

DDO 154

DDO 154 is a gas dominated nearby dwarf galaxy. This galaxy is classified as Irregular Barred galaxy or IB(s) (de Vaucouleurs et al. 1991). A distance of 4.3 Mpc derived from brightest blue stars by Karachentsev et al. (2004) was adopted for this study. This is consistent with the previous results adopted in the literature (Carignan & Beaulieu 1989; Carignan & Freeman 1988). The first HI observation of this galaxy was done in November 1985 (Carignan & Freeman 1988). DDO 154 is part of the THINGS. The kinematics and rotation curves of 19 galaxies from THINGS were derived by de Blok et al. (2008) and these are the highest quality rotation curves available to date. The inclination and Position Angle are shown in table 1.

IC 2574

IC 2574 is a spiral galaxy in the constellation of Ursa Major. It is classified as SAB(s)m according to the RC3 catalog (de Vaucouleurs et al. 1991). This galaxy is at a distance of 4.02 Mpc derived from the brightest blue stars (Karachentsev et al. 2004). The rotation curves from THINGS were used to do the mass model. Gentile et al. (2011) mentioned that the HI gas of this galaxy contains holes and shells.

NGC 925

This galaxy is a barred spiral galaxy in the constellation of Triangulum classified as SAB(s)d (de Vaucouleurs et al. 1991). The gas distribution of NGC 925 also has holes and shells which are seen in the gas rotation curves. The galaxy has been observed at 21 cm for more than forty years, with single dish (Höglund & Roberts 1965; Gottesman 1980) and with interferometer arrays (Pisano et al. 1998; Walter et al. 2008). The data from (Walter et al. 2008) is the most recent observation for this galaxy, the rotation curves were derived by de Blok et al. (2008). NGC 925 is part of the Hubble Space Telescope key project to measure the Hubble constant , thus the cepheid distance of 9.16 Mpc reported in Freedman et al. (2001) is adopted.

NGC 2366

NGC 2366 is a dwarf galaxy and a member of the M81 group. Oh et al. (2008) derived the rotation curves of this galaxy, the non-circular motions also were investigated. As listed in Table 1, a cepheid distance of 3.44 Mpc (Tolstoy et al. 1995) is adopted.

NGC 2403

This galaxy belongs also to the M81 group of galaxies.
It is classified as a barred spiral galaxy SAB(s)cd according to the de Vaucouleurs

classification scheme (de Vaucouleurs et al. 1991). NGC 2403 is a well known bright spiral galaxy. It has been extensively used to test MOND. For example NGC 2403 was part of the sample of Begeman et al. (1991) to estimate the value of the MOND acceleration parameter. The most recent rotation curve of NGC 2403 was derived by de Blok et al. (2008). NGC 2403 is also part of the sample by Gentile et al. (2011) in the context of MOND. A cepheid distance of 3.22 Mpc is adopted for this work (Freedman et al. 2001).

NGC 2841

NGC 2841 is classified as SA(s)b (de Vaucouleurs et al. 1991) and located in the constellation of Ursa Major. It has a cepheid distance of 14.1 Mpc (Freedman et al. 2001). The adopted distance plays a very important rule for this galaxy. Begeman et al. (1991) mentioned that an acceptable fit is obtained if the distance is twice as much as the Hubble distance of 9.46 Mpc. When the cepheid distance is used, a large M/L is needed to produce an acceptable fit to the rotation curve which is in contradiction with observation. However, Gentile et al. (2011) have pointed out that this galaxy would not be problematic for MOND if the cepheid distance of 14.1 Mpc is adopted and the simple μ-function is used instead of the standard μ-function. We adopted the same distance of 14.1 Mpc for this study.

NGC 3031

NGC 3031 or M81 is a bright spiral galaxy in the constellation of Ursa Major. NGC 3031 is located at a distance of 3.63 Mpc Freedman et al. (2001). The existence of non-circular motions is reported by de Blok et al. (2008). For this reason it is excluded from the Gentile et al. (2011) sample and the observed rotation curve has not yet been confronted with the MOND formalism. Trachternach et al. (2008) quantified the non-circular motions for this galaxy and found that they lie between 3 and 15 km s^{-1} for an average of 9 km s^{-1}. They also noticed that the outer disk

is warped and that there is some disturbance in the velocity field.

NGC 3198

This is a grand design spiral galaxy in the constellation of Ursa Major. The cepheid distance of 13.80 Mpc of Freedman et al. (2001) is used in this work . NGC 3198 has been used extensively in the literatures in the context of MOND. These studies led to the same conclusion that NGC 3198 might be problematic for MOND. It would need a much lower distance compared to the cepheid distance of 13.8 Mpc if the standard value for a_0 was adopted (Begeman et al. 1991).

NGC 3621

NGC 3621 is classified as SA(s)d galaxy (de Vaucouleurs et al. 1991). It is located at a distance of 6.64 Mpc in the constellation of Hydra Freedman et al. (2001). It is a well behaved galaxy with a flat rotation curve up to very large radii. Among the cepheid distance determination for NGC 3621 are 6.3 ± 0.7 Mpc (Rawson et al. 1997) and 6.6 ± 0.46 Mpc Freedman et al. (2001). These are in good agreement within their adopted error bars. Both MOND and dark matter halos models produced very good fits to the rotation curves of this galaxy.

NGC 7331

NGC 7331 is a spiral galaxy in the constellation of Pegasus, it is classified as SA(s)b. A cepheid distance of 14.72 Mpc (Freedman et al. 2001) is adopted in this study. The HI rotation curve of NGC 7331 have been confronted in the context of MOND by Begeman et al. (1991) derived from VLA observations and in Gentile et al. (2011) from THINGS data (Walter et al. 2008). Here we use a combined H_α and HI rotation curves to enhanced the resolution of the rotation curves in the inner parts.

NGC 7793

NGC 7793 is a member of the Sculptor Group, it is classified as S(s)d (de Vaucouleurs et al. 1991). The most recent cepheid distance for NGC 7793 is 3.43 Mpc. This was measured as part of the Araucaria Project (Gieren et al. 2005). The rotation curve derived from the THINGS data is used in this study.

2.2.2 Sculptor Group Galaxies

NGC 55

NGC 55 is a barred spiral SB(s)m (de Vaucouleurs et al. 1991) galaxy member of the Sculptor group consisting of about 30 galaxies. A cepheid distance of 1.9 Mpc was measured by Gieren et al. (2008) as part the Araucaria Project. The HI rotation curve was derived by Puche & Carignan (1991) from VLA observations.

NGC 247

NGC 247 is a nearby dwarf galaxy part of the Sculptor group of galaxy. This galaxy is classified as SB(s)cd (de Vaucouleurs et al. 1991). The most recent cepheid distance for NGC 247 is 3.4 Mpc. This was measured as part of the Araucaria Project (Gieren et al. 2009). The rotation curve of NGC 247 was taken from Carignan & Puche (1990).

NGC 300

NGC 300 is a well known spiral galaxy part of the Sculptor Group classified as SA(s)d. This galaxy has been observed at 21 cm wavelength using the 27.4 m twin-element interferometer of the Owen Valley Radio Observatory (Rogstad et al. 1979), using the Very large Array with the D and C configuration (Puche & Carignan 1991). The latest HI observation of NGC 300 was done with the Australian Compact

Array telescope (Westmeier et al. 2011). The HI rotation curves in Westmeier et al. (2011) was chosen from this analysis because it is more extended compared to the one done by Puche & Carignan (1991) derived from VLA data. A cepheid distance of 1.99 Mpc was measured using 19 cepheid variables Gieren et al. (2005). This is adopted in this study.

2.2.3 NGC 3109

NGC 3109 is a nearby dwarf galaxy located at a distance of about 1.30 Mpc from us. It is classified as SB(s)m according to the classification scheme proposed by de Vaucouleurs et al. (1991). The first cepheid distance of NGC 3109 was measured by Gieren et al. (2005) from a total of 19 cepheid variables. The HI rotation curves presented in Jobin & Carignan (1990) will be used for this galaxy. This was derived from a VLA observation using C and D configurations. Another HI observation were done using the 64 m Parkes telescope in Australia (Barnes & de Blok 2001), but they could not derive the rotation curve because of the lack of spatial resolution. Begeman et al. (1991) noticed that the gas component need to be increased by a factor of 1.67 after a comparison with single dish observations in the 21 cm wavelength to be in accord with MOND.

Chapter 3

Mass Model

3.1 Mass Model with Dark Matter Halos

The mass model is done by comparing the observed rotation curves of the galaxy to the calculated rotation curves of all the components (gas, stars and dark matter) derived from the observed mass distribution. It is well known that neutral hydrogen has a larger radial extent compared to the luminous part of the galaxy. Therefore the rotation curve derived using the HI gas traces most of the mass of the galaxy out to very large radii. The rotation curves of all the components are required for the mass model. The components needed to do the model are the baryonic (stars and gas) component and the dark matter component. The stellar components were derived from the 3.6 microns surface brightness profiles and were converted into mass using the mass-to-light ratio (M/L) which is the factor used to convert luminosity density into mass density. This M/L is assumed to be constant with radius. The 3.6 microns band is less affected by dust extinction, and moreover probes the old stellar population which represents the bulk of the stellar content of the galaxy. The 3.6 microns band can also contain some Polycyclic Aromatic Hydrocarbons (PAHs) and Asymptotic Giant Branch (AGB) stars which are tracers of emission from hot dust (Trachternach et al. 2008). Most of the gas content of the

galaxy is in the form of neutral hydrogen, thus the gas contribution is derived from the HI map corrected for the primordial helium contribution. The dark matter halo component is derived from a theoretical density profile which needs to be defined. The mass model was performed using the following formula

$$V_{rot}^2 = V_{gas}^2 + V_*^2 + V_{halo}^2 \tag{14}$$

where V_{gas} is the gas contribution to the rotation curves, V_* the contribution from the stars and V_{halo} from the dark matter component.

The main contribution to the rotation curves are from the dark matter component, therefore, the choice of the density profile is very important. There are many dark matter halo profiles presented in the literature. These profiles can be summarised into two groups (Oh et al. 2008): the core-central density group and the cusp central density group. The cored group are well represented by the ISO halo and the cusp group represented by the Navarro-Frenk-White (NFW) dark matter halo profile.

3.1.1 The pseudo-Isothermal Dark Matter Halo Model (ISO)

The pseudo-Isothermal dark matter halo is an observationally motivated model with a constant central-density core. The mass distribution is given by:

$$\rho_{ISO}(R) = \frac{\rho_0}{1 + (\frac{R}{R_c})^2} \tag{15}$$

where ρ_0 is the central density and R_c the core radius. The corresponding rotation curves is given by:

$$V_{ISO}(R) = \sqrt{4\pi G \rho_0 R_C^2 [1 - \frac{R}{R_C} atan(\frac{R}{R_C})]} \tag{16}$$

where ρ_0 and R_C are the central density and the core radius of the halo, respectively.

3.1.2 The Navarro, Frenk and White Dark Matter Halo Model (NFW)

The NFW profile is also known as the "universal density profile" (Navarro et al. 1997). It is the commonly adopted dark matter halo profile in the context of ΛCDM cosmology. It was derived from N-body simulations.
The density profile is given by:

$$\rho_{NFW}(R) = \frac{\rho_i}{R/R_S(1+R/R_S)^2} \tag{17}$$

Where ρ_i is the density of the universe when the dark matter collapse and R_c a scale radius.

The corresponding rotation curves reads

$$V_{NFW}(R) = V_{200}\sqrt{\frac{ln(1+cx) - cx/(1+cx)}{x[ln(1+c) - c/(1+c)]}} \tag{18}$$

where c is the parameter quantifying the degree of concentration of the DM halo. V_{200} is the rotation velocity at radius R_{200} where the density contrast with the critical density of the universe exceeds 200 and x is defined as R/R_{200}.

3.1.3 The Einasto Dark Matter Halo Model

It has been shown that the model with a finite central density core is in better agreement with the observations compared to the cusp model predicted by simulations (Begeman et al. 1991; de Blok et al. 2008). Prompted by the work of Fukushige & Makino (2001) who argued that the NFW halo model underestimates the amount of dark matter in the inner regions of a galaxy, Navarro et al. (2004) introduced a new model which gives a much better fit to the rotation curves than the NFW model. Merritt et al. (2006) considered this model and found that it was originally proposed by Einasto (1969) for the distribution of mass in galaxies. The density

profile is given by:

$$\rho_E(R) = \rho_{-2} exp(-2n[(\frac{R}{R_{-2}})^{\frac{1}{n}} - 1]) \tag{19}$$

where, R_{-2} is the radius where the density prole has a logarithm slope of -2 , ρ_{-2} is the local density at that radius and n is the Einasto index .

Following the method described by Mamon & Łokas (2005) and with some little algebra, the corresponding rotation curves reads

$$V_E(R) = \sqrt{4\pi G R_{-2}^3 n(2n)^{-3n} exp(2n) \frac{1}{R}[\Gamma(3n) - \Gamma(3n, R/R_{-2})]} \tag{20}$$

where $\Gamma(x)$ is the incomplete gamma function

$$\Gamma(3n, x) = \int_0^x e^{-t} t^{3n-1} dt$$

3.2 Modified Newtonian Dynamics

Modified Newtonian Dynamics (MOND) was proposed by Milgrom (1983b) as an alternative to dark matter. Therefore, in the MOND formalism only the rotation curves of the gas component and stellar component are required to explain the observed rotation curves. In 1983, Milgrom presented a modification of newtonian dynamics in his three series of papers. MOND is based on the following assumptions:

- Standard dynamics breakdown in the limit of small accelerations
- The acceleration of a test particle, in a gravitating system, is given by $\mu(\mathrm{g}/\mathrm{a}_0) \times \mathbf{g} \simeq \mathbf{g}_N$, where $\mathbf{g}_N$ is the Newtonian gravitational acceleration.
- The acceleration constant a_0 determine the transition from the Newtonian regime to the low acceleration asymptotic regime.

The shape of the predicted MOND rotation curves depends on the interpolating function. The standard and simple interpolating function are mostly used in the literature. The standard μ-function is the original form of the interpolating function

proposed by Milgrom (1983b) but Zhao & Famaey (2006) found that a simplified form of the interpolating function provides good fits to the observed rotation curves and the derived mass-to-light ratio are more compatible with those obtained with stellar synthesis models when this function is used.

The MOND rotation curves are estimated from equation 4. For the standard μ-function the derivation of the rotation curves is presented in Swaters et al. (2010) and also shown in the next sections.

3.2.1 MOND rotation curves using the standard interpolating function

The MOND formula is:

$$\mu(x = g/a_0)g = g_N \tag{21}$$

The standard interpolating function is given as

$$\mu(x) = \frac{x}{\sqrt{1+x^2}} \tag{22}$$

where x have an asymptotic behaviour, for x $\ll$ 1 the system is in deep MOND regime with g = $(g_N a_0)^{1/2}$ and for x$\gg$ 1 the gravity is Newtonian. By putting g in the equation 4 and with some algebra the MOND rotation curve reads:

$$V_{rot}^2 = \frac{V_{sum}^2}{\sqrt{2}}\sqrt{1+\sqrt{1+(2ra_0/V_{sum}^2)^2}} \tag{23}$$

Where

$$V_{sum}^2 = V_b^2 + V_d^2 + V_g^2 \tag{24}$$

where V_d, V_b, V_g are the contribution from the stellar disk, bulge and the gas to the rotation curves. In this work, the stellar contribution was not decomposed into bulge and stellar disk component. That is to minimize the number of free parameter involve in the mass models. The other reason is that the bulge-disc decomposition could also introduce additional uncertainties on the stellar contribution.

3.2.2 MOND Rotation Curves with the Simple Interpolating Function

The simple interpolating function is given by

$$\mu(x) = \frac{x}{1+x} \tag{25}$$

Using the same procedure as in previous section we can easily obtain the corresponding rotation velocity

$$V_{rot}^2 = \sqrt{V_b^2 + V_d^2 + V_g^2} * \sqrt{a_0 * r + V_b^2 + V_d^2 + V_g^2} \tag{26}$$

3.2.3 Mass Model using GIPSY

GIPSY is an acronym for Groningen Image Processing System (van der Hulst et al. 1992). GIPSY is a software package designed to reduce and manipulate astronomical data. The tasks for the mass model are ROTMOD and ROTMAS. ROTMAS is the main task for the mass model. It is an interactive task which was designed to fit the rotation curves calculated from the different components (gas, stars and dark matter halo) to an observed rotation curves. The routines use a least square algorithm to estimate the unknown parameters. ROTMAS has three variable parameters namely mb, md and mg which are the mass scaling factors for the stellar bulge, the stellar disk and the gas component. The other free parameters comes from the adopted dark matter halo density profile. For a mass model using MOND, the acceleration parameter a_0 could be taken as a free parameter. The fitting results are written on the screen and also stored in the GIPSY log file and the data can be saved on disk.

The gas and stellar contributions were calculated using ROTMOD. Mass density profiles derived from the HI distribution maps corrected for the Helium contribution were used for the gas component and the 3.6 microns surface brightness profile for the stellar component. ROTMOD calculates the rotation curves for a tracunted

exponential disk for a given density profile (Casertano 1983). In this paper, Casertano proposed a method to estimate the contribution to the rotation curves from the different components (stars, gas and dark matter halo). He stipulated that their might be a similarity between the luminosity distribution and the mass density distribution in galaxies. Therefore, he calculated the mass density profile of the stars using the following equations:

$$\rho(r,z) = \rho_0(r)[ch(\frac{z}{z_0})]^2 \tag{27}$$

where z_0 is the disk scale height and ρ_0(r) the central density of an exponential disk in units of $M_\odot$ pc^{-2} with

$$\rho_0(r) = \begin{array}{ll} \rho_{00}(r)exp(-r/h) & (r \leqslant R) \\ \rho_0(R)[1-(r-R)/\delta] & (R \leqslant r \leqslant R+\delta) \\ 0 & (R+\delta \leqslant r) \end{array} \tag{28}$$

where R is the cutoff radius, δ the cutoff length and h the disk scale length in kpc. A trancuted exponential disk is characterized by equation 27 & 28.
There are two possible ways to enter the mass density distribution in ROTMOD:

- the mass density profile is used when available, ROTMOD estimates the total mass (e.g total HI mass or stellar mass) in $M_\odot$ and calculates its contribution to the rotation curves from the given density profile. When the radii are not in physical units the distance to the galaxy also must be provided.

- if the density profile is not available, then, the parameters which define each components must be given. These parameters are: The total mass in solar masses, the central density ρ_0, the scale length h and the cutoff radius R_{cutoff}.

The outputs from the task ROTMOD were used as inputs for the task rotmas. A Screenshot for the GIPSY task ROTMOD is shown in figure 5, the top panel is for the bulge, middle panel for the stellar disk and bottom panel for the gas component.

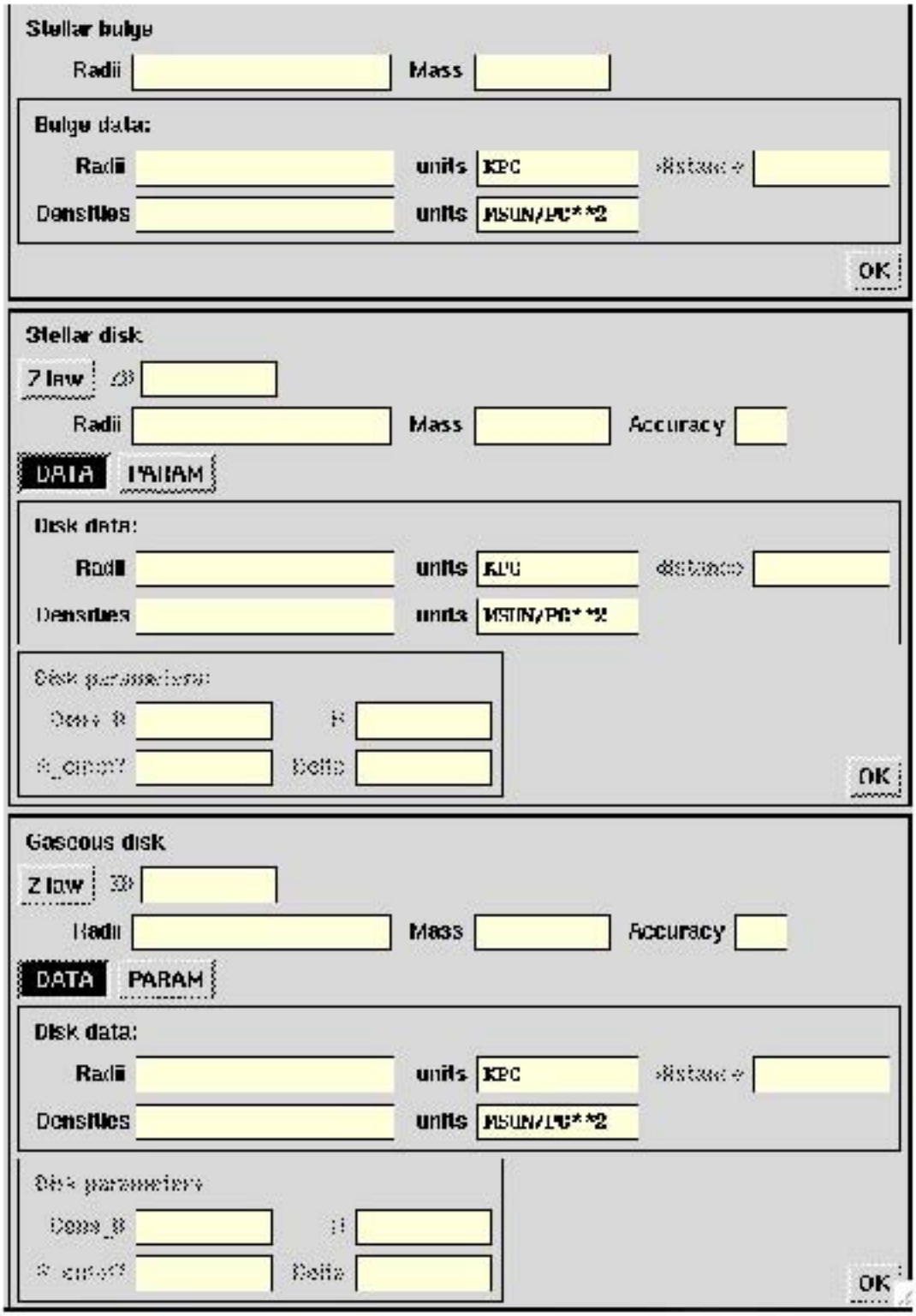

Figure 5: Image of the GIPSY task ROTMOD, this task was used to compute the gas and stellar contribution to the rotation curve from a given density profiles, the top panel is for the stellar bulge component, the middle panel for the stellar disk component and the bottom panel for the gas component, the outputs from this task are used for the task ROTMAS.

3.3 Gas and Stellar Contributions

3.3.1 Gas Contribution

The HI gas from VLA observations using the combined B, C and D array configurations (Walter et al. 2008) were used to compute the mass density profile of the gas. The gas density profile is computed using the GIPSY task ELLINT using the tilted ring parameters from de Blok et al. (2008). The HI gas is corrected by a factor of 1.4 for Helium and other metals contributions. The output from ELLINT is then used in ROTMOD to calculate the gas contribution for the mass model by assuming an infinitely thin disk. For NGC 300 the HI gas was taken from Westmeier et al. (2011) which is the most recent data available for this galaxy, derived from HI observation using the Australia Telescope Compact Array with a 8.8 km s^{-1} velocity resolution. The rotation curves and the gas density profile of NGC 3109 are presented in Jobin & Carignan (1990) which were derived from VLA HI observations. The gas mass density, the inclination and the position angle of the remaining galaxies are collected from the literature (cf table 1).

3.3.2 Stellar Contribution

In order to minimise the errors in the mass models, the 3.6 microns surface brightness profiles were used for the stellar contribution (de Blok et al. 2008). The 3.6 micron probes most of the emission from old stellar population (Verheijen 1997). The surface brightness profile of the THINGS sample were derived by de Blok (private communication). The profiles were corrected for inclination before being converted into mass density. We followed the method in Oh et al. (2008) to convert the luminosity profiles into mass density profiles. Oh et al. (2008) first converted the surface brightness profile in mag/arcsec^2 into a luminosity density profile in units of $L_\odot/pc^2$ and then converted to mass density using the following equation:

$$\Sigma[M_\odot pc^{-2}] = \Upsilon_*^{3.6} \times 10^{-0.4\times(\mu_{3.6}-C^{3.6})} \quad (29)$$

where $\Upsilon_*^{3.6}$ is the stellar-mass-to-light ratio in the 3.6 micron band, $\mu_{3.6}$ the surface brightness profile and $C^{3.6}$ is a constant used for the conversion from mag/arcsec^2 to $L_\odot/pc^2$. The details to find $C^{3.6}$ is presented in Oh et al. (2008), it is given by:

$$C^{3.6} = M_\odot^{3.6} + 21.56 \tag{30}$$

Where $M_\odot^{3.6}$ is the absolute magnitude of the sun in the 3.6 micron band. Using the distance modulus formula and the distance to the sun Oh et al. (2008) found:

$$M_\odot^{3.6} = m_\odot^{3.6} + 31.57 = 3.24 \tag{31}$$

The stellar mass-to-light ratio was left as a free parameter. However, a prior value is needed to convert the luminosity density in units of $L_\odot/pc^2$ into mass density profile in unit of $M_\odot/pc^2$. M/L from de Blok et al. (2008) derived using the Kroupa Initial Mass Function (IMF) were used for the galaxies that form part of the THINGS sample, for the remaining galaxies, the M/L were collected from the literature.

3.3.3 Gas and Stellar Contribution for NGC 247

Surface brightness profiles of NGC 247 in the optical B band and the 3.6 microns band are shown in Figure 6. The B-band profile was derived from Schmidt plates by Carignan (1985b). The 3.6 microns profile were derived from IRAC image retrieved from the archives. Bright stars in the vicinity of the galaxy were removed by hand before the image was fitted with ellipses using the IRAF task ELLIPSE. The mean intensity for each ellipse were converted into surface brightness following the method described in section 3.3.2 for the stellar contribution (see also Oh et al. (2008)). A pixel size of 1.2 arcsec/pixel was used to convert from pixel into arcsecond.

Figure 7 shows the HI gas density profile of NGC 247 corrected for the primordial Helium contribution. This profile was derived from VLA observations by Carignan (1990).

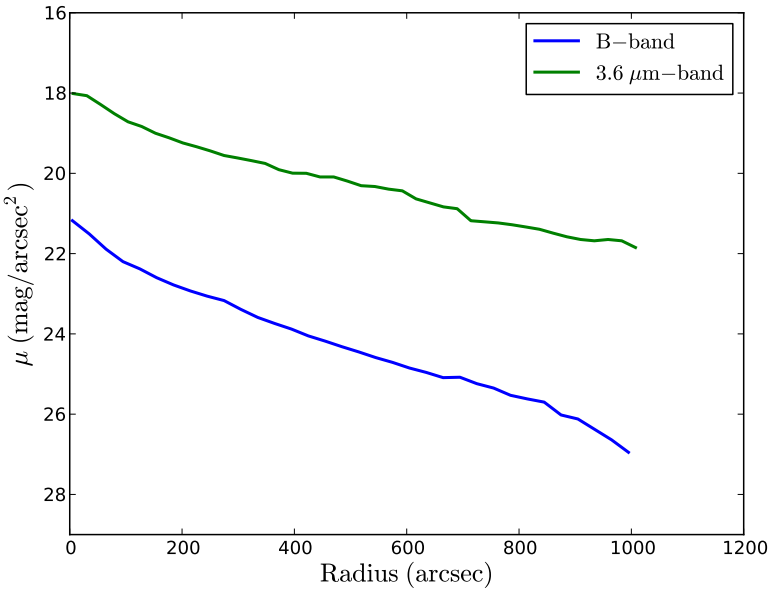

Figure 6: Plot of the B and 3.6 microns surface brightness profiles of NGC 247 (B band profile taken from Carignan (1985a)

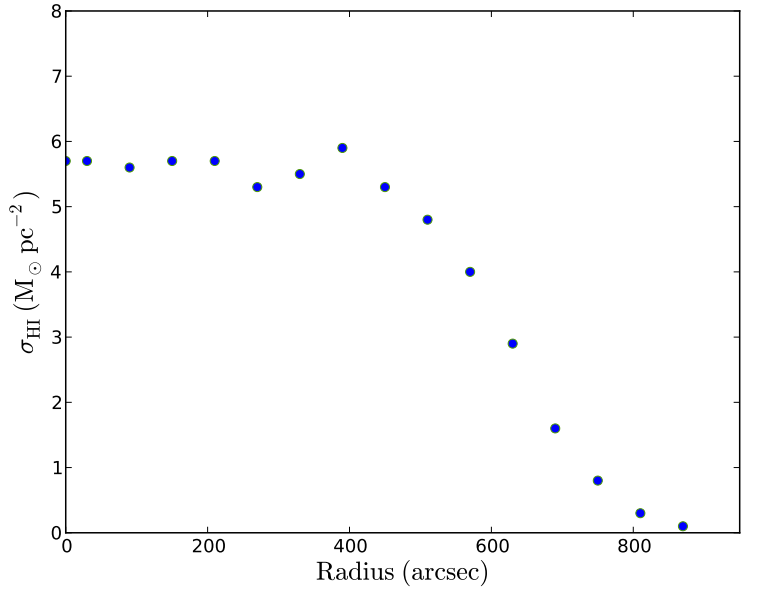

Figure 7: NGC 247 HI gas density profile corrected for the helium contribution (taken from Carignan (1990))

3.4 Resampled THINGS Rotation Curves

The rotation curves of the galaxies part of The HI Nearby Galaxy Survey (THINGS) (Walter et al. 2008) were derived by de Blok et al. (2008) from HI observation with the Very Large Array in B, C and D configurations. The rotation curves were sampled with two data points per spatial resolution element. This did not allow de Blok et al. (2008) to make a direct comparison between the ISO halo and the NFW halo. Therefore, we used a resampled version of THINGS rotation curves which will allow us to make a qualitative comparison between the models. This also is needed in order to have a more homogenous sample because the rest of the galaxies in the sample have rotation curves derived using only one data point per spatial resolution element. In this way, all the data points are independant. This was firstly suggested by Chemin et al. (2011) for their analysis of the THINGS rotation curves derived by de Blok et al. (2008) using the Einasto halo model. They found that the resulting χ^2 are more significant and could be used as a direct comparison when a resampled version of the rotation curves was used.

Chapter 4

Results & Discussions

4.1 Extrapolated Central Surface Brightness and Disk Scale Length

One of the aims of this work is to find any correlation between the MOND acceleration constant a_0 and other parameters of the galaxy such as absolute magnitude and central surface brightness. Therefore, the 3.6 micron extrapolated surface brightness and disk scale length were derived for our sample galaxies. The 3.6 microns surface brightness profiles of the galaxies part of THINGS were derived by de Blok (private communication) using Sptizer 3.6 microns images. The central surface brightness and the disk scale length were obtained by fitting the profile with an exponential disk given by equation 24. The results for the central surface brightness and disk scale length in the 3.6 microns are presented in Table 2 where col.1 is the galaxy name, col.2 is the corrected extrapolated central surface brightness and cols.3 and 4 are the disk scale lengths in arcsecs and kpc.

$$\mu_{3.6} = \mu_{3.6}(0) + 1.085 * (r/\alpha^{-1}) \tag{32}$$

Table 2: Central surface brightness and disk scale length of the galaxies in our sample

Galaxy	$\mu_{3.6}(0)_c$ mag/arcsec^2	$\alpha_{3.6}^{-1}$ arcsec	$\alpha_{3.6}^{-1}$ kpc
1	2	3	4
DDO 154	21.15 ± 0.05	46.87 ± 1.51	0.97 ± 0.03
IC 2574	19.79 ± 0.02	129.35 ± 0.61	2.51 ± 0.02
NGC 0247	19.94 ± 0.03	215.83 ± 1.62	3.55 ± 0.03
NGC 0925	18.61 ± 0.12	93.00 ± 2.73	2.91 ± 0.12
NGC 2366	20.50 ± 0.04	114.72 ± 1.65	1.91 ± 0.02
NGC 2403	18.32 ± 0.08	132.93 ± 2.95	2.05 ± 0.05
NGC 2841	16.41 ± 0.09	59.15 ± 0.92	4.03 ± 0.06
NGC 3031	16.42 ± 0.03	152.17 ± 1.21	2.67 ± 0.02
NGC 3198	18.74 ± 0.18	54.95 ± 1.68	3.66 ± 0.11
NGC 3621	16.71 ± 0.06	72.13 ± 1.22	2.32 ± 0.04
NGC 7331	16.29 ± 0.07	67.15 ± 1.33	4.78 ± 0.09
NGC 7793	17.10 ± 0.06	67.39 ± 0.98	1.12 ± 0.02

4.2 Mass Model Results

The gas and stellar contributions to the rotation curves were computed with the GIPSY task ROTMOD. The outputs from ROTMOD were used in ROTMAS which is the main task for the mass model. ROTMAS uses a non-linear least square method and compares the observed rotation curves to the calculated rotation curves derived from the observed mass distribution of the gas and stars. Inverse squared weighting of the rotation curves with the uncertainties were used during the fitting procedure. We performed MOND fits where M/L is the free parameter and derived two sets of fits. Firstly, with a_0 fixed using the standard value $a_0 = 1.21 \times 10^{-8}$ cm s^{-2} derived by Begeman et al. (1991). Secondly, with a_0 as a free parameter, this will allow us to find the value giving the best fit and to look for any systematic trends. Furthermore, this will allow to identify galaxies in which a_0 exhibits a significant departure from the standard value. We also performed mass model with ISO and NFW dark matter halos for our sample galaxies with fixed M/L assuming a Kroupa IMF. M/L were derived following the method described in Chapter 3 (see also: Oh et al. 2008). Finally, mass models using Einasto halos were derived for our sample galaxies with the help of Laurent Chemin. Two sets of fits were made, with M/L fixed and free.

4.2.1 One and Two Parameters MOND Fit Results

MOND fits with one and two parameters are shown in Figure 8 to 12. One parameter fits results with a_0 fixed and M/L free are shown on the left panels and the two parameter fits with M/L and a_0 free on the right panels. The observed rotation curves are shown as points and the MOND rotation curves calculated from the observed mass density distribution of the stars and gas in continuous bold lines. The stellar contributions are shown as dashed lines and the gas contribution as long-dashed lines. Results for the one parameter and two parameters MOND fits

are summarised in Table 3. The first column is galaxy name, mass-to-light ratio and the reduced chi-squared for a_0 fixed results for the one parameter fits are shown in columns 2 and 3. The result for the two parameter fits are in columns 5, 6 and 7. We found an average value of a_0 of 1.12 $\pm$ 0.10 10^{-8} cm s^{-2} using the standard interpolating function. This value is consistent with Begeman et al. (1991). However, two galaxies (NGC 7793 and NGC 925) required a_0 two times larger than the standard value and smaller values for NGC 247 and NGC 3031. More details about the galaxies which show discrepancies between the rotation curve predicted by MOND and the observed rotation curve will be given in the discussion section.

4.2.2 ISO and NFW Dark Matter Halos Fit Results

Mass model results using the ISO dark matter halo and the NFW halo models are shown in Figure 13 to 17. The ISO halo fit results are shown on the left panels and NFW halo fit results on the right panels. The dark matter halo components are shown as dotted-dashed lines, the contribution from the stellar component as dashed lines and from the gas component as long-dashed lines. The parameter results are summarised in Table 4.

Figure 13 to 17 show that the ISO dark matter halo model ($< \chi_r^2 > = 1.94$, NGC 7793 excluded) produces much better fits to the rotation curves compared to the cusp NFW halo model ($< \chi_r^2 > = 2.16$, NGC 7793 excluded), this is consistent with previous studies (e.g. de Blok et al. 2008).

4.2.3 Einasto Dark Matter Halo Model Fit Results

As discussed in chapter 3, the Einasto halo model is an improved version of NFW. The shape of the rotation curves of the Einasto halo model depends on its index n. Models with $n > 4$ correspond to a cusp central density and $n < 4$ to a cored central density. The results for the Einasto models are shown in figure 18 and 20 for fixed M/L. The M/L with Kroupa Initial Mass Function (IMF) from de Blok

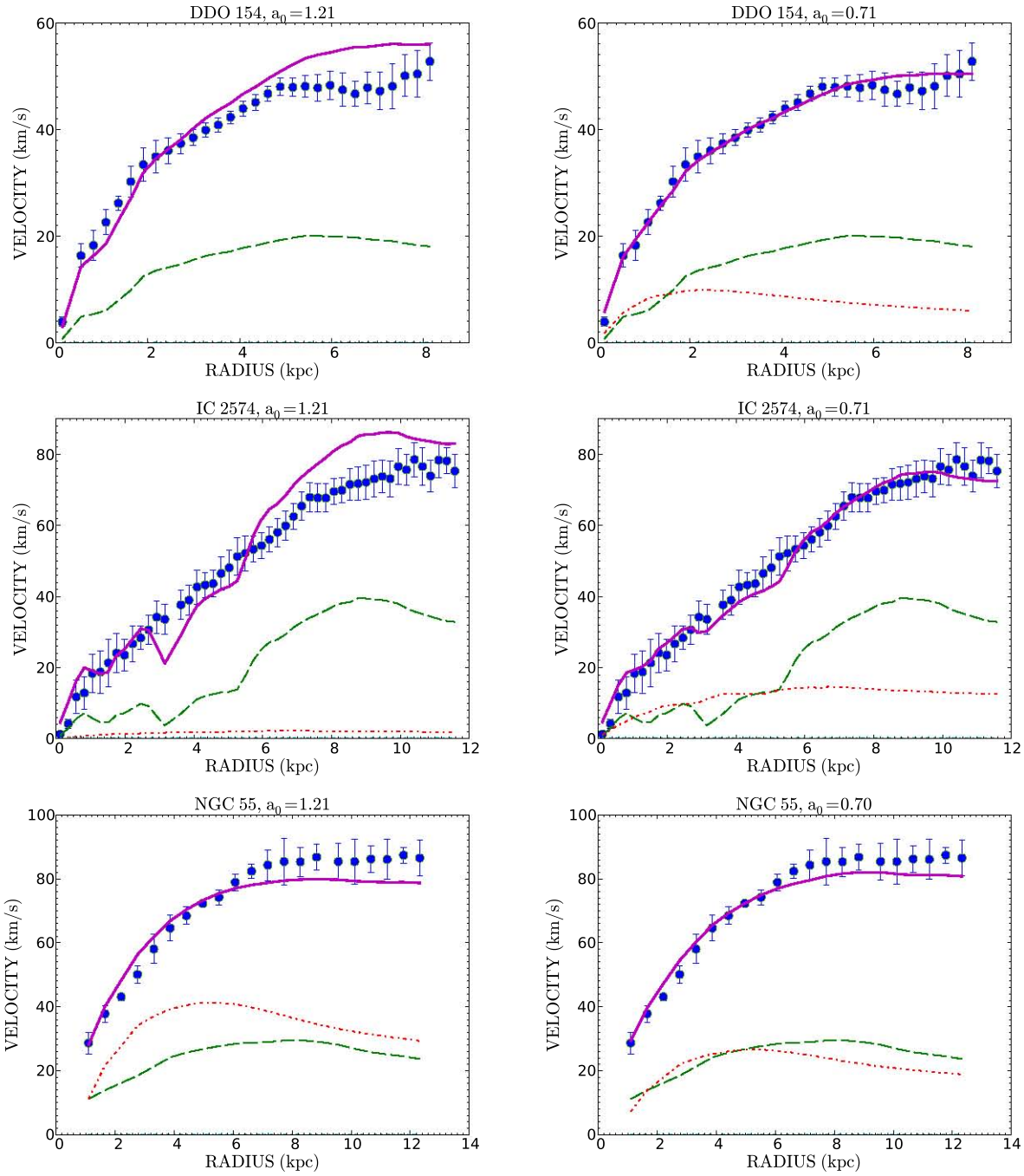

Figure 8: MOND rotation curves fitting results; Left panel: MOND fits with a_0 fixed, Right panel: MOND fits with a_0 free. The value of a_0 shown on the graphs are in units of 10^{-8} $cm\ s^{-2}$. The dashed lines are the contributions from the stars to the rotation curves and the long-dashed lines from the gas. The best fitting results are presented in bold lines and the observed rotation curves as points.

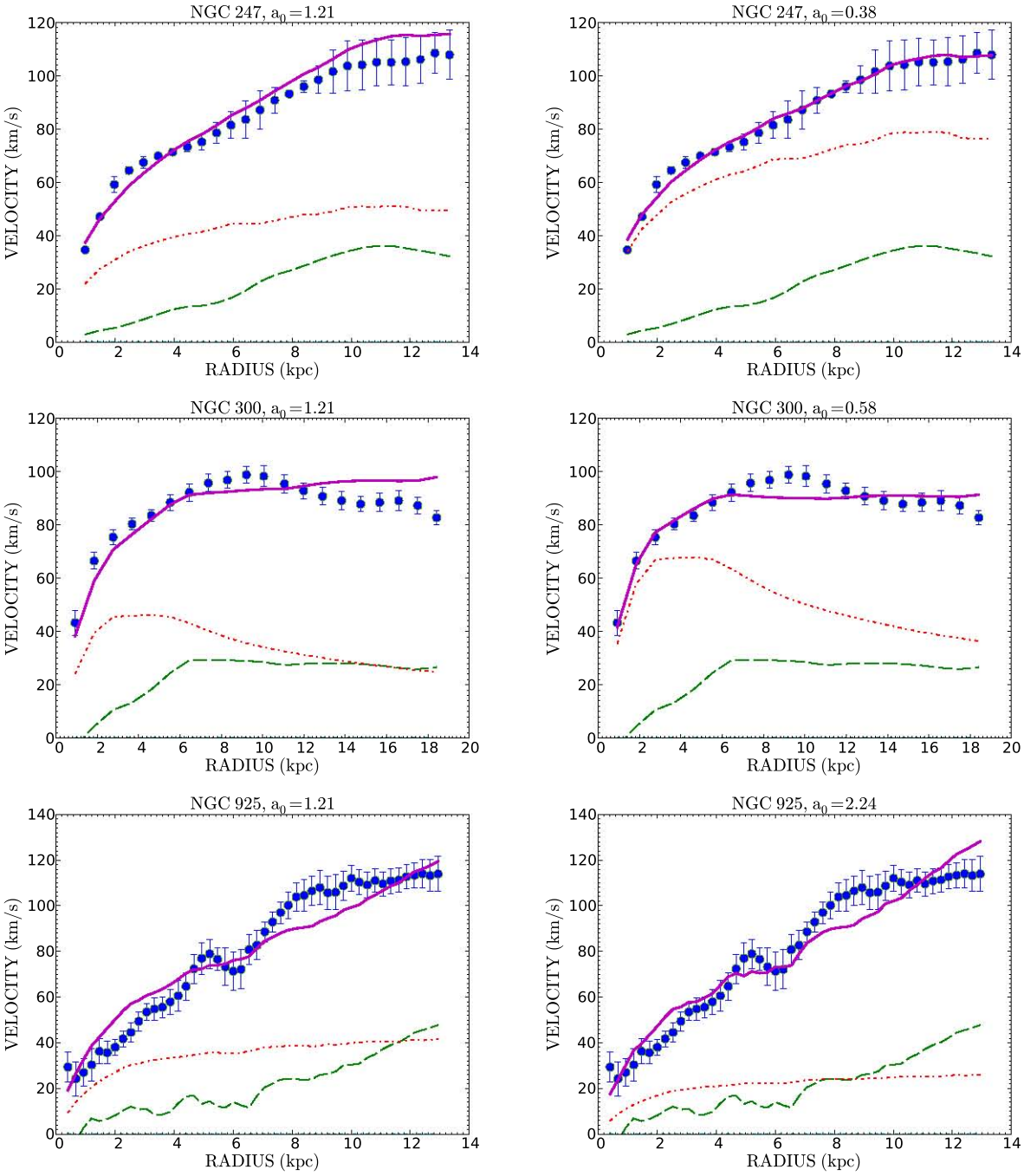

Figure 9: MOND rotation curves fits results (continued)

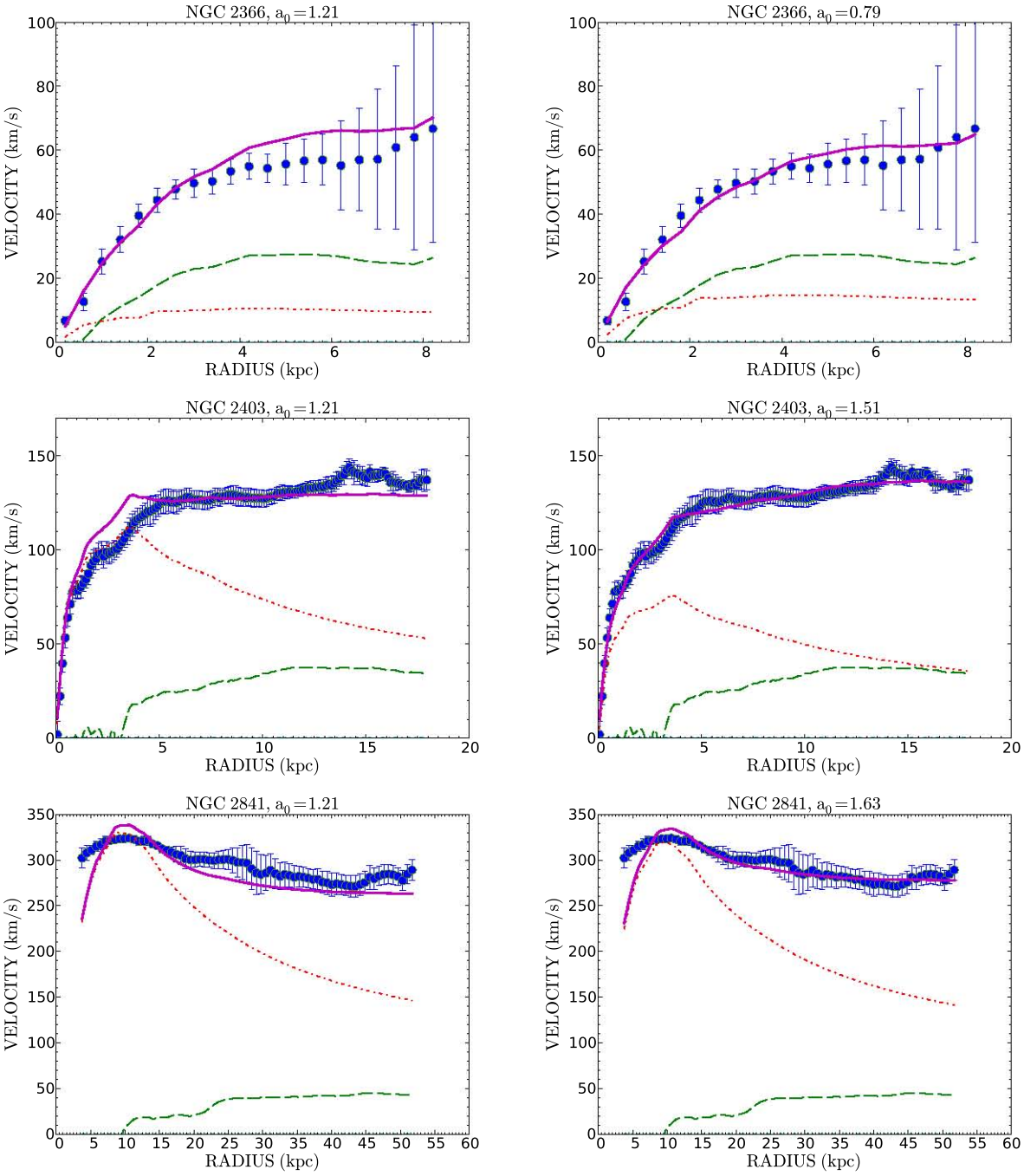

Figure 10: MOND rotation curves fits results (continued)

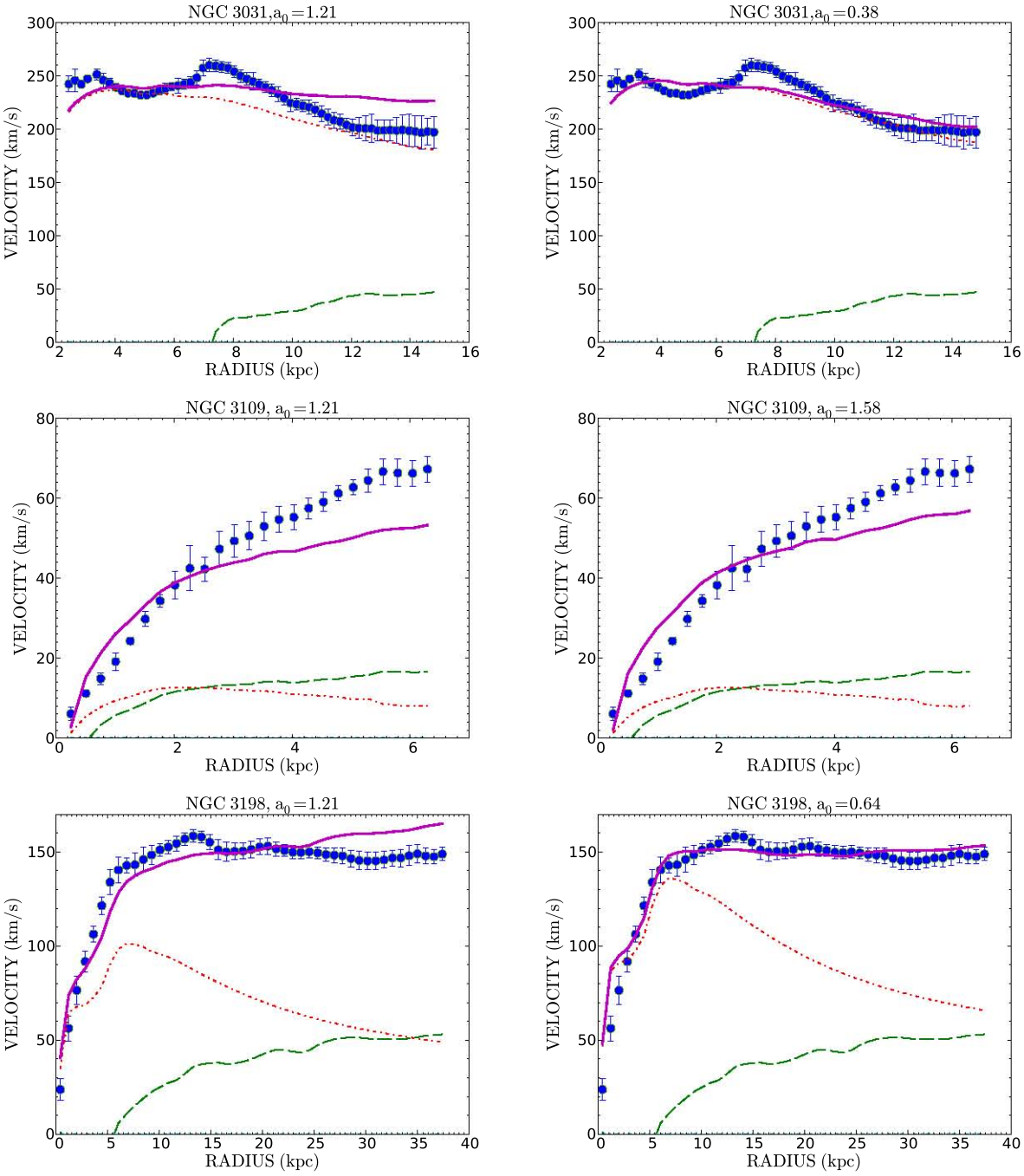

Figure 11: MOND rotation curves fits results (continued)

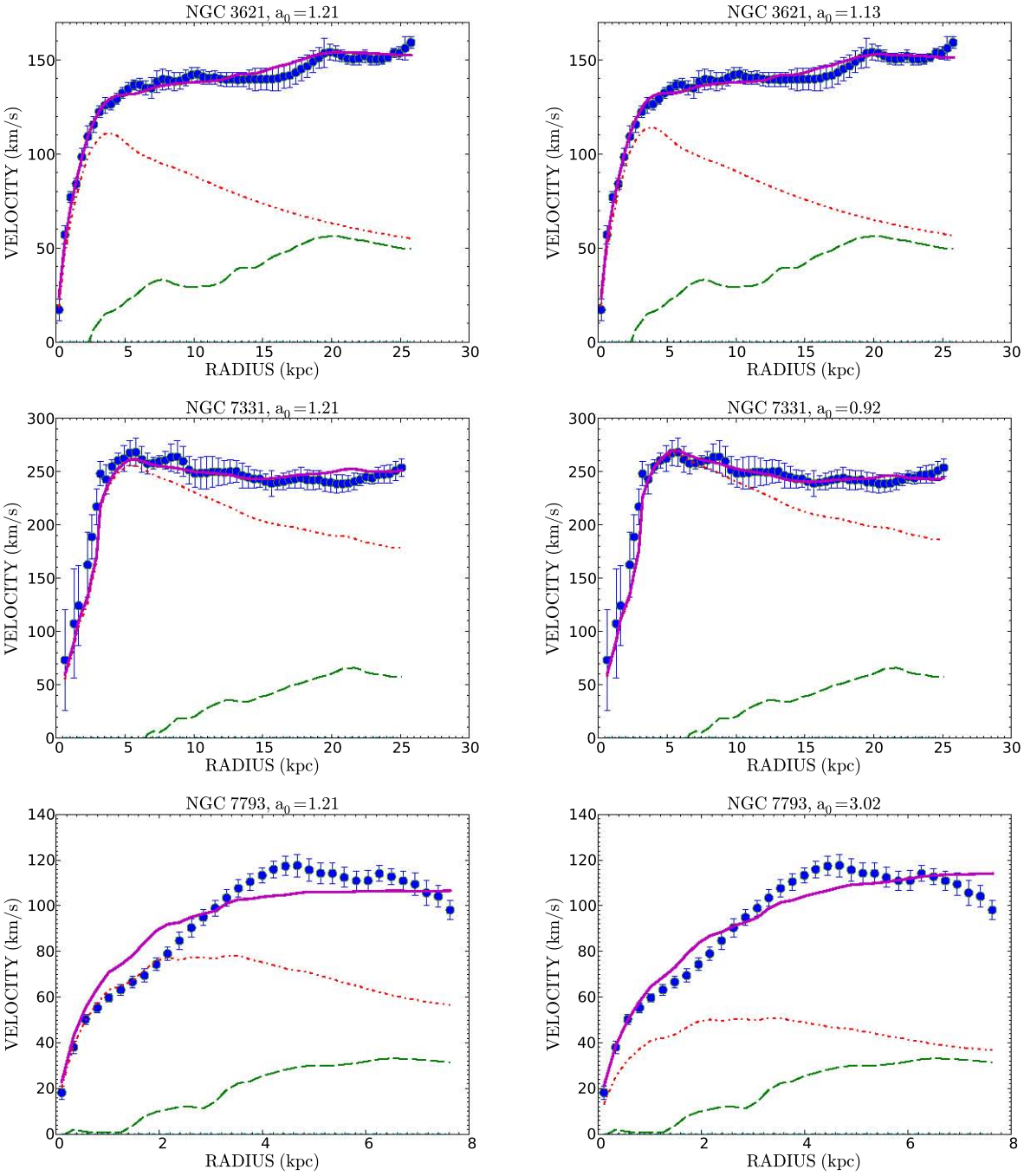

Figure 12: MOND rotation curves fits results (continued)

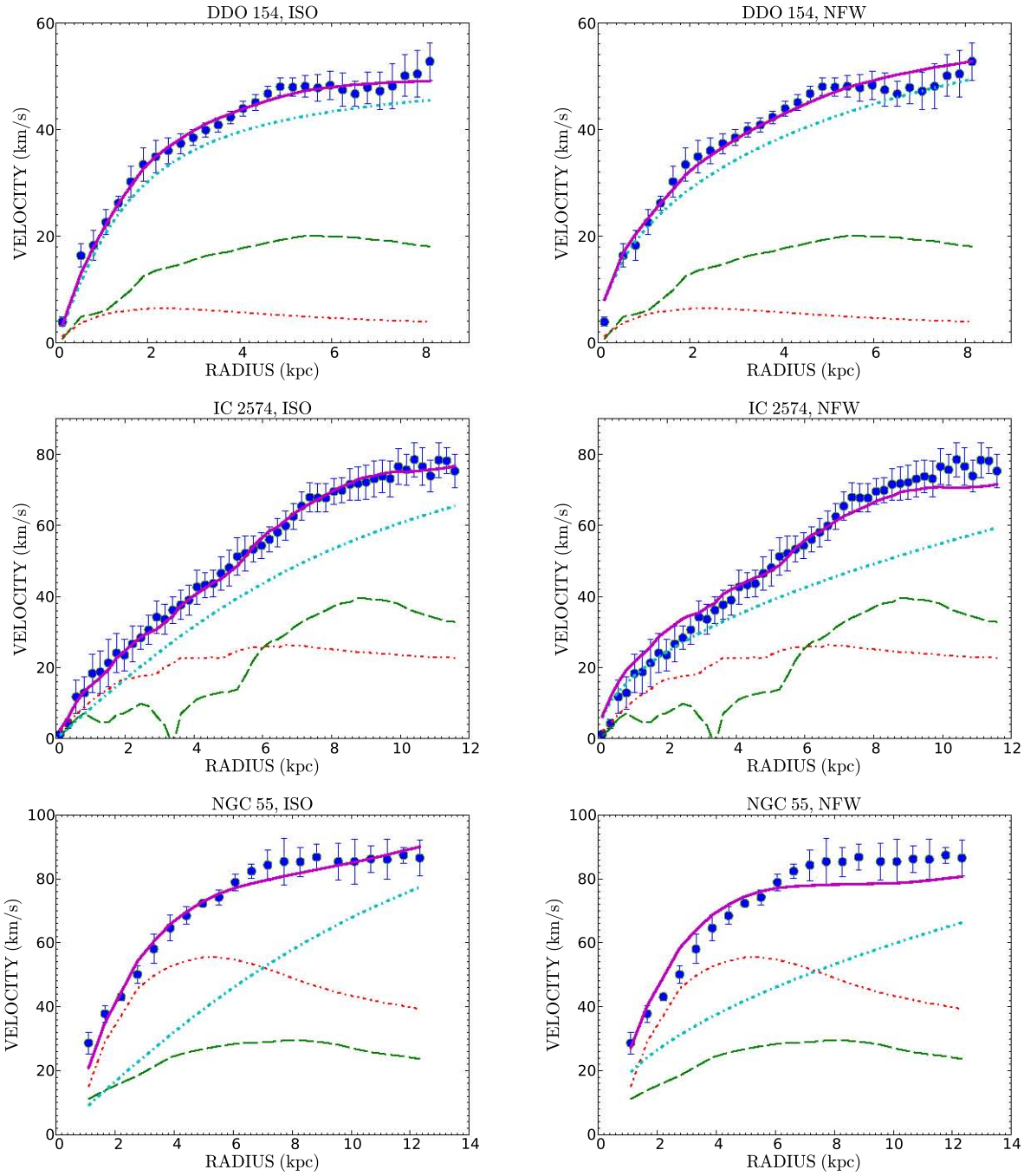

Figure 13: Mass model results using the ISO and NFW dark matter halos. The dashed lines represent the contribution from the stars to the rotation curves, the long-dashed lines the ones for the gas and the doted dashed lines the contribution from the dark matter halo. The best fitting results are presented in bold lines and the observed rotation curves as points

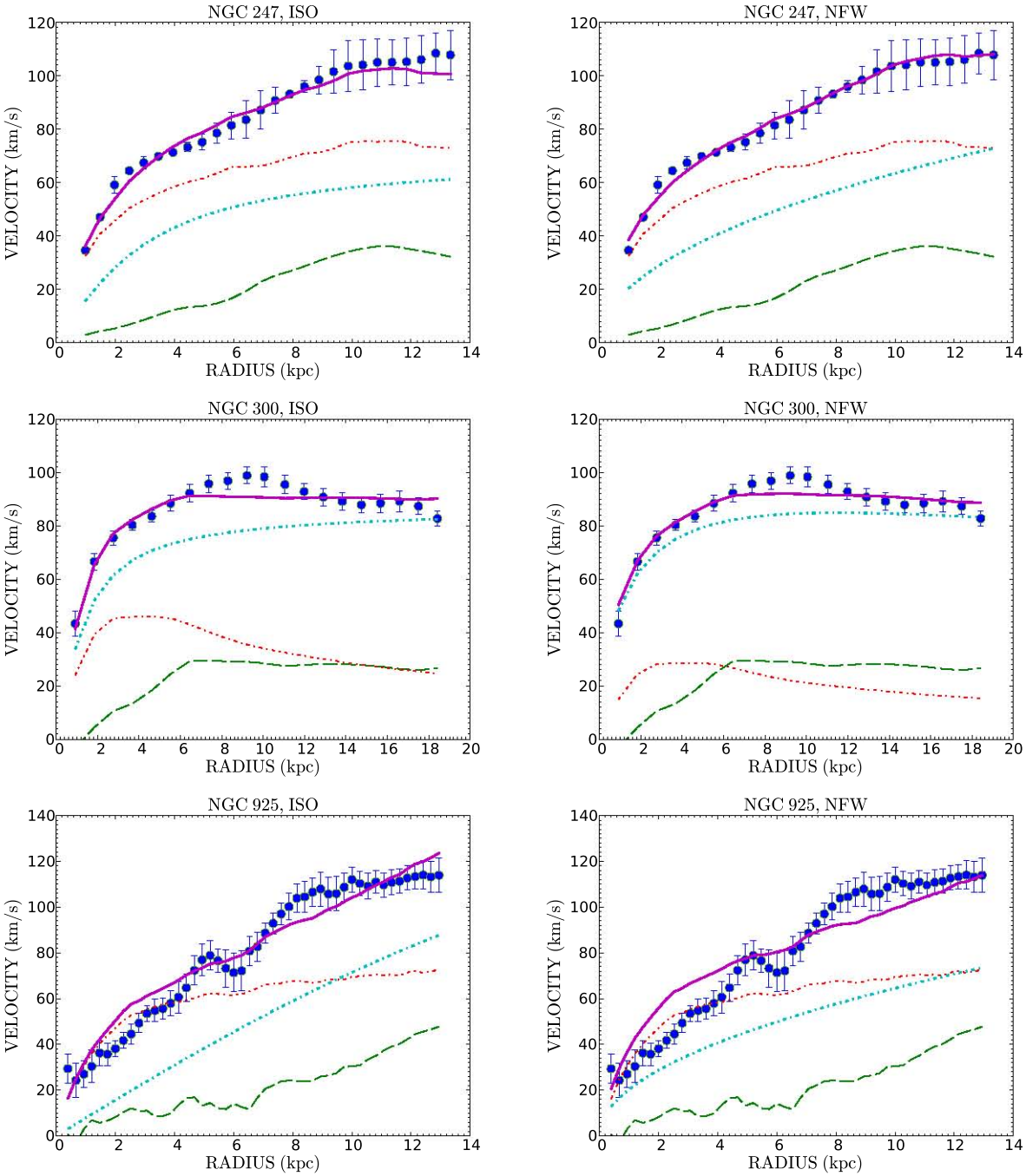

Figure 14: Mass model results using the ISO and NFW dark matter halos (continued)

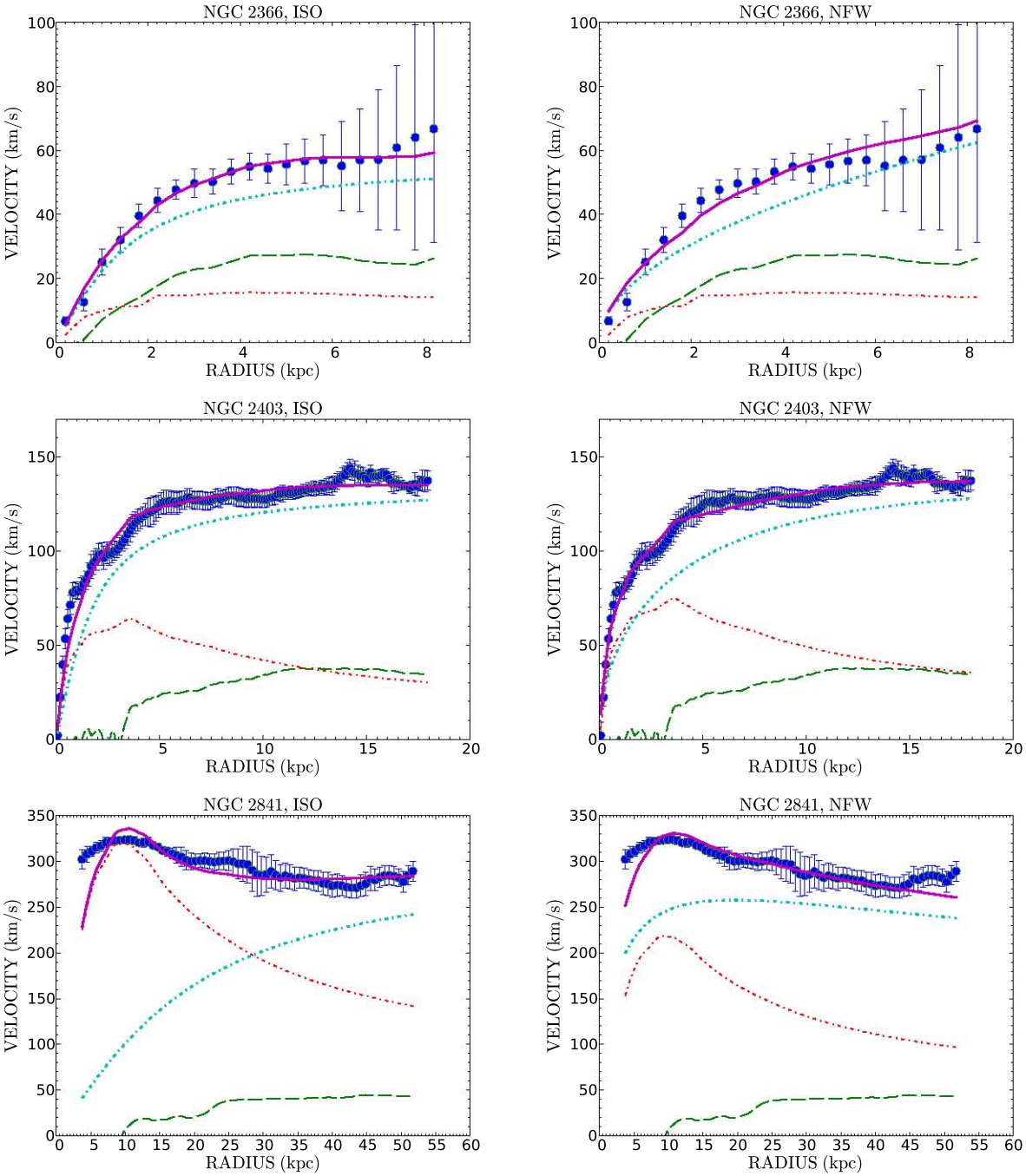

Figure 15: Mass model results using the ISO and NFW dark matter halos (continued)

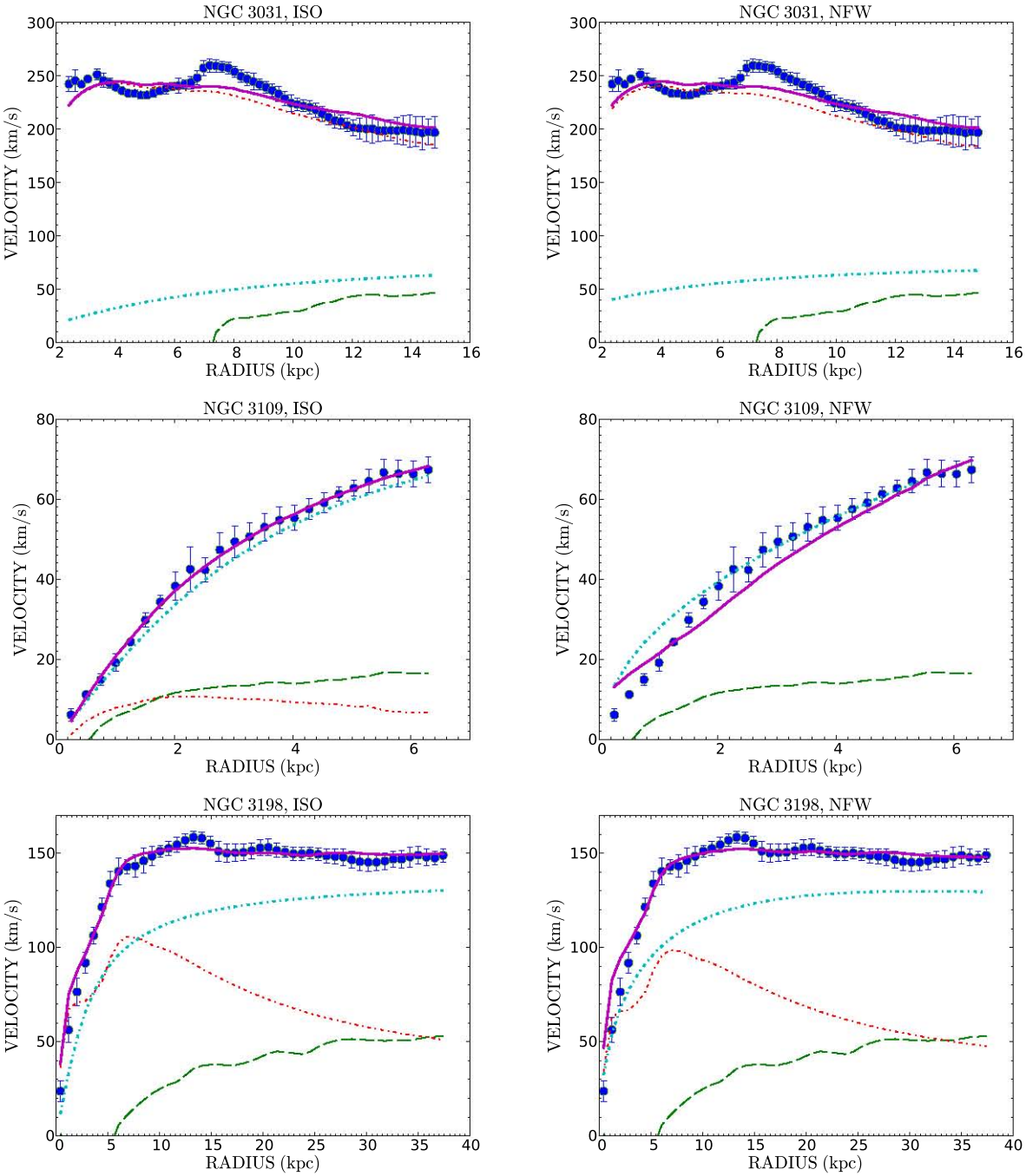

Figure 16: Mass model results using the ISO and NFW dark matter halos (continued)

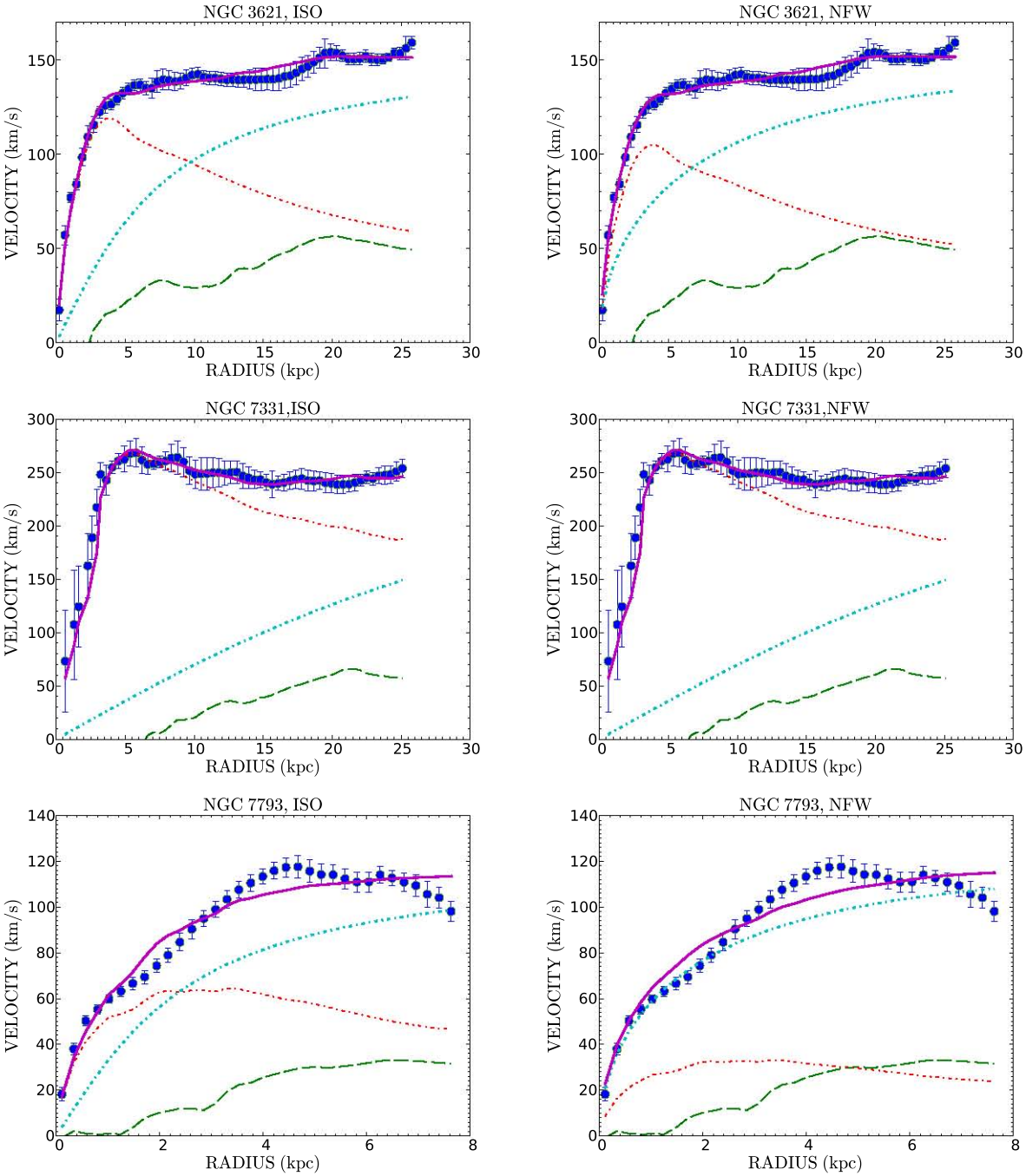

Figure 17: Mass model results using the ISO and NFW dark matter halos (continued)

Table 3: Mass models using the MOND formalism with a_0 fixed (1.21×10^{-8} cm s^{-2}) and a_0 free .

	a_0 fixed		a_0 free		
Name	$(M/L)_*$	χ^2_r	$(M/L)_*$	a_0 10^{-8} cm s^{-2}	χ^2_r
1	2	3	4	5	6
DD0 154	-	3.61	0.54	0.70 ±0.04	0.46
IC 2574	-	4.39	0.10	0.61 ± 0.06	1.44
NGC 0055	0.21	1.61	0.50	0.70 ± 0.04	2.86
NGC 0247	0.14	2.82	0.34	0.38 ± 0.10	1.71
NGC 0300	0.61	4.71	1.30	0.58 ± 0.08	2.13
NGC 0925	0.16	2.43	0.10	2.24 ± 0.33	2.05
NGC 2366	0.12	0.85	0.21	0.79 ± 0.10	0.42
NGC 2403	0.89	3.31	0.41	1.51 ± 0.07	0.54
NGC 2841	1.21	4.09	1.13	1.63 ± 0.10	2.98
NGC 3031	0.73	5.26	0.79	0.38 ± 0.16	3.49
NGC 3109	0.10	14.56	0.11	1.58 ±0.26	13.57
NGC 3198	0.37	5.68	0.66	0.64 ± 0.04	2.03
NGC 3621	0.38	0.65	0.40	1.13 ± 0.03	0.59
NGC 7331	0.59	0.81	0.64	0.92 ± 0.04	0.41
NGC 7793	0.38	70.65	0.16	3.02 ± 0.65	44.91
		<3.91 >*		<1.01 ± 0.10 >	<2.47 >*

*Mean of the reduced chi-squared excluding NGC 7793
col. 1: Galaxy name
col. 2 & 4: mass-to-light ratio of the stellar disks
col. 3 & 6: reduced chi-squared
col. 5: MOND acceleration parameter

Table 4: Mass model results for the ISO and NFW dark matter halo models

	NFW			ISO		
Name	c	V_{200} km s^{-1}	χ^2_r kpc	R_C $M_\odot$ pc^{-3}	ρ_0	χ^2_r
1	2	3	4	5	6	7
DD0 154	2.3 ± 0.4	64 ±8	1.28	1.3±0.1	27.11±2.1	0.39
IC 2574	<0.1	>500	2.59	7.3±0.5	4.1±0.2	1.22
NGC 0055	<0.1	>500	4.13	10.2±1.6	3.8 ± 0.3	0.95
NGC 0247	0.4 ±1.2	189 ±204	1.72	2.4 ±0.5	15.1 ±27.5	1.24
NGC 0300	9.7 ±3.1	70 ±2	1.36	1.1±0.4	100.4 ± 73.1	1.88
NGC 0925	<0.1	>500	4.26	16.6±10.1	3.4 ± 0.7	2.09
NGC 2366	<0.1	>500	0.99	1.2±0.1	37.4 ± 4.2	0.20
NGC 2403	6.1± 0.4	120±2	0.56	1.5±0.1	153.8 ± 10.7	1.05
NGC 2841	15.4±0.6	192±3	2.20	16.1±3.4	6.8 ± 1.9	3.48
NGC 3031	3.5±31.2	69±110	3.43	3.6±31.2	50.8± 80.65	3.43
NGC 3109	<0.1	561±43	5.33	2.95±0.33	19.50 ±2.6	0.24
NGC 3198	6.1±1.6	119±3	1.37	2.7±0.4	48.1 ± 16.6	0.84
NGC 3621	3.7±0.3	139±4	0.59	6.1±0.4	12.5±1.5	0.69
NGC 7331	<0.1	68±28	0.42	26.8±10.1	2.8±0.6	0.44
NGC 7793	9.4±11.5	95±35	53.35	1.9±0.8	68.4±45.6	40.17
			<2.2 >*			<1.9 >*

*Mean of the reduced chi-squared excluding NGC 7793
col. 1: Galaxy name
col. 2: NFW halo concentration
col. 3: NFW halo characteristic velocity
col. 4: NFW reduced chi-squared
col. 5: ISO halo core radius
col. 6: ISO halo central density
col. 7: ISO reduced chi-squared.

(2008) were used from the galaxies part of THINGS and those from the original papers for the remaining galaxies. The results with M/L free are shown in figure 21 and 23. The points with errorbars represent the observed rotation curves. The best fits Einasto halo model are shown as solid line, the dark matter halo component as dotted dashed lines, the stellar component as dashed lines and the gas component as double dotted dashed lines. The parameters results are presented in Table 5 for M/L fixed and Table 6 for M/L free.

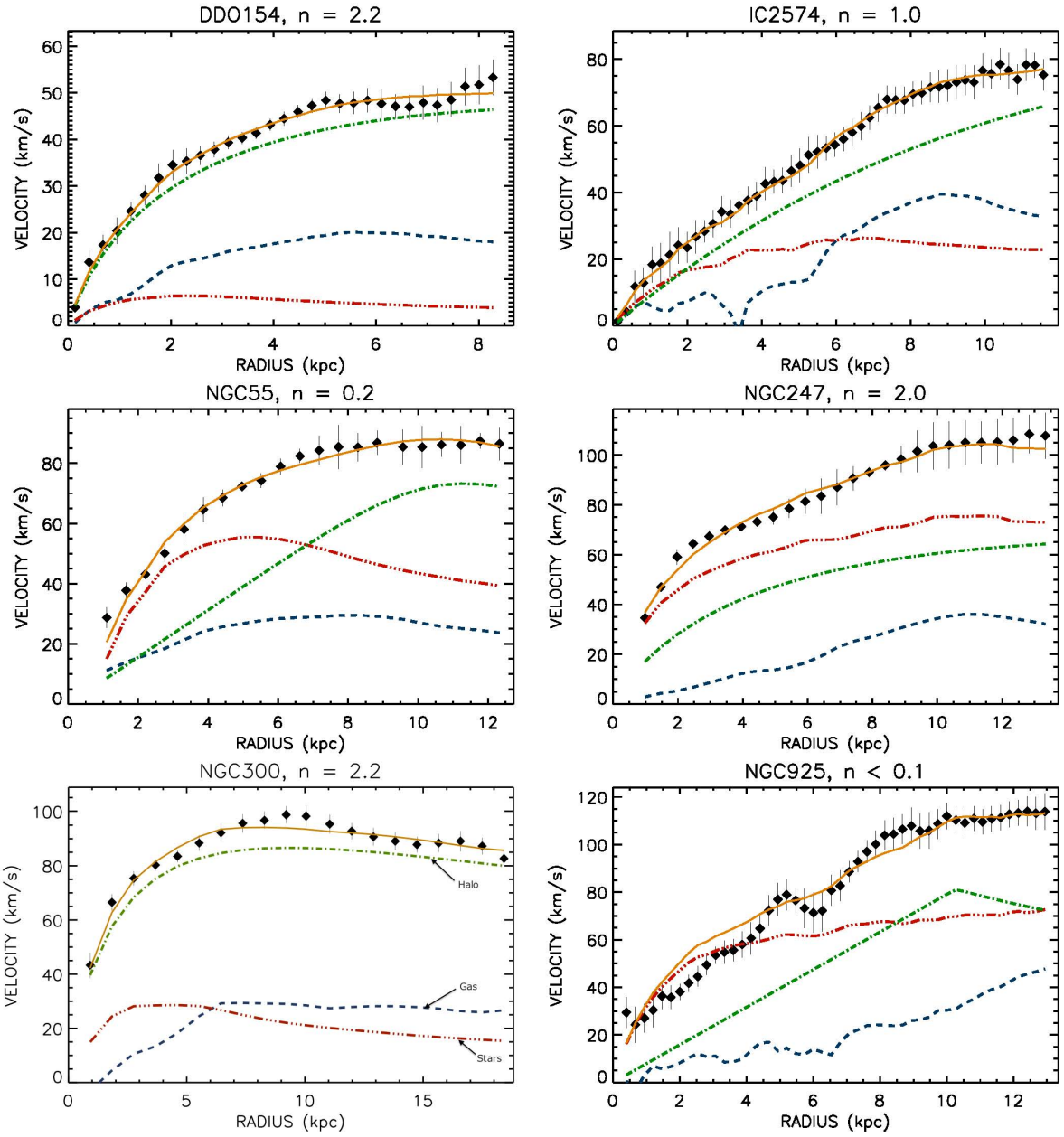

Figure 18: Mass model results using the Einasto DM halo model with M/L fixed. The doted lines are the contributions from the stars and dark matter halo to the rotation curves and the dashed lines are from the gas contribution. The best fitting results are presented in bold lines and the observed rotation curves as points.

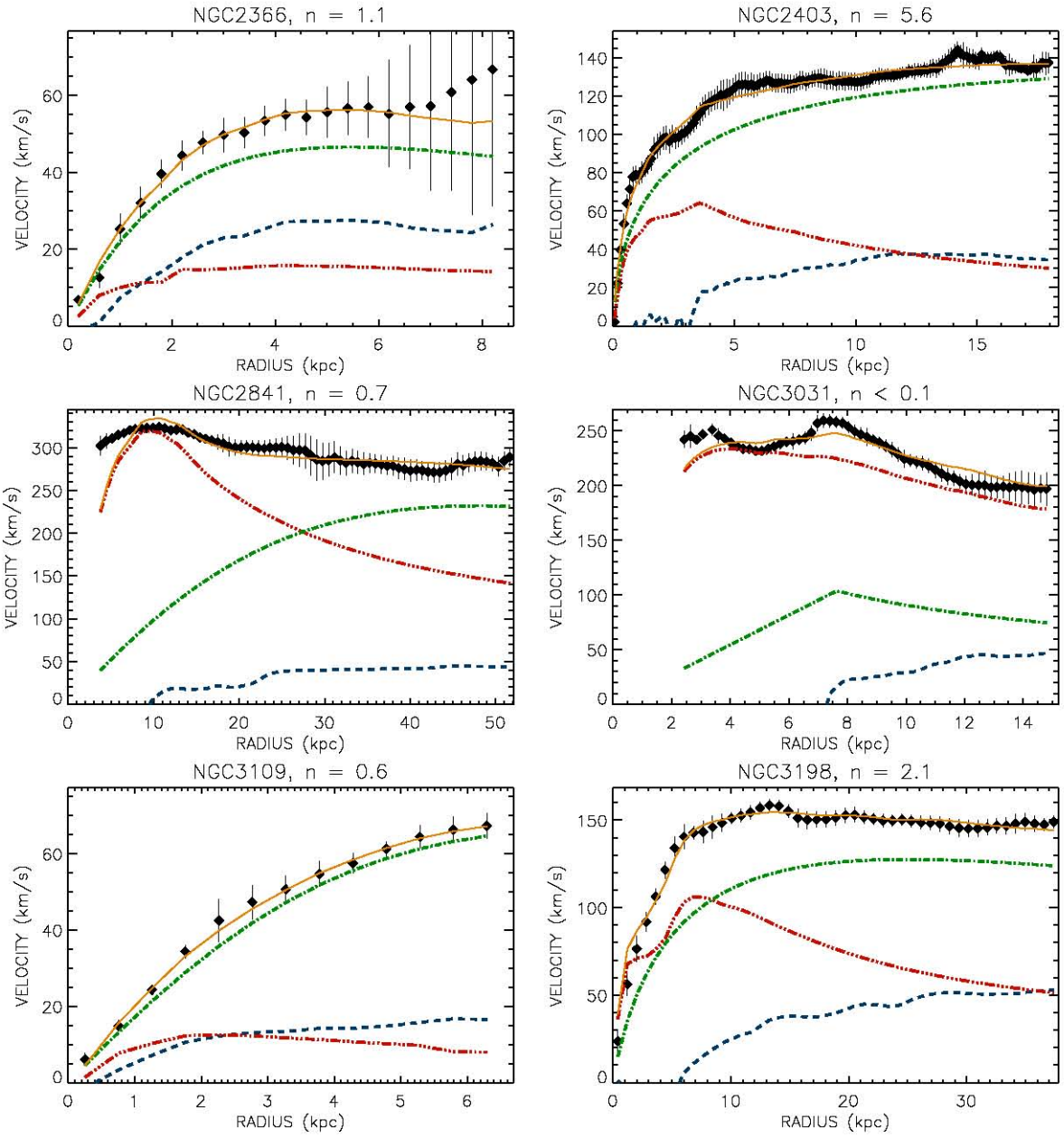

Figure 19: Mass model results using Einasto DM halo model with M/L fixed (continued)

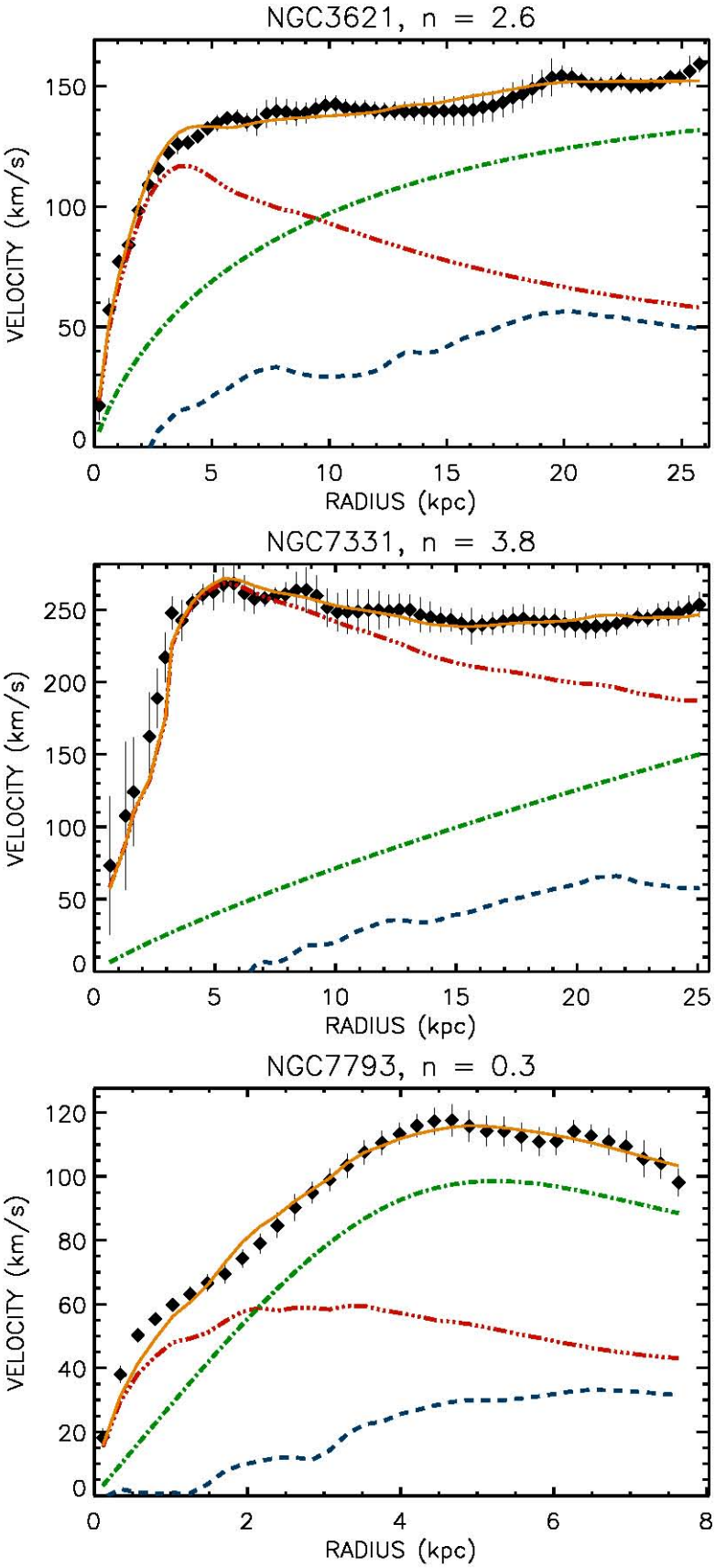

Figure 20: Mass model results using Einasto DM halo model with M/L fixed (continued)

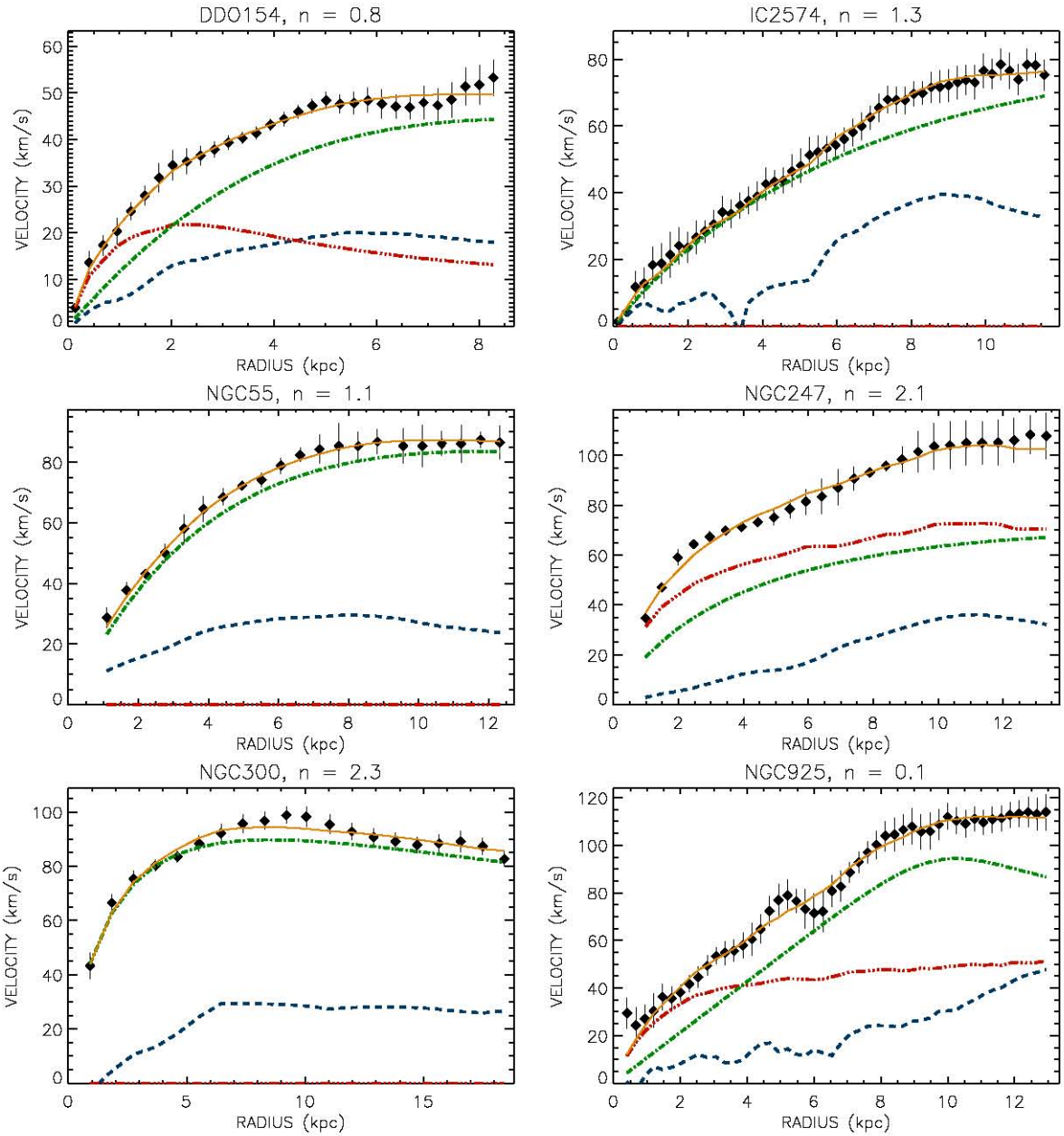

Figure 21: Mass model results using the Einasto DM halo model with M/L free. The dashed lines are the contributions from the stars to the rotation curves, the long-dashed lines from the gas and the doted dashed lines from the dark matter halo. The best fitting results are presented in bold lines and the observed rotation curves as points.

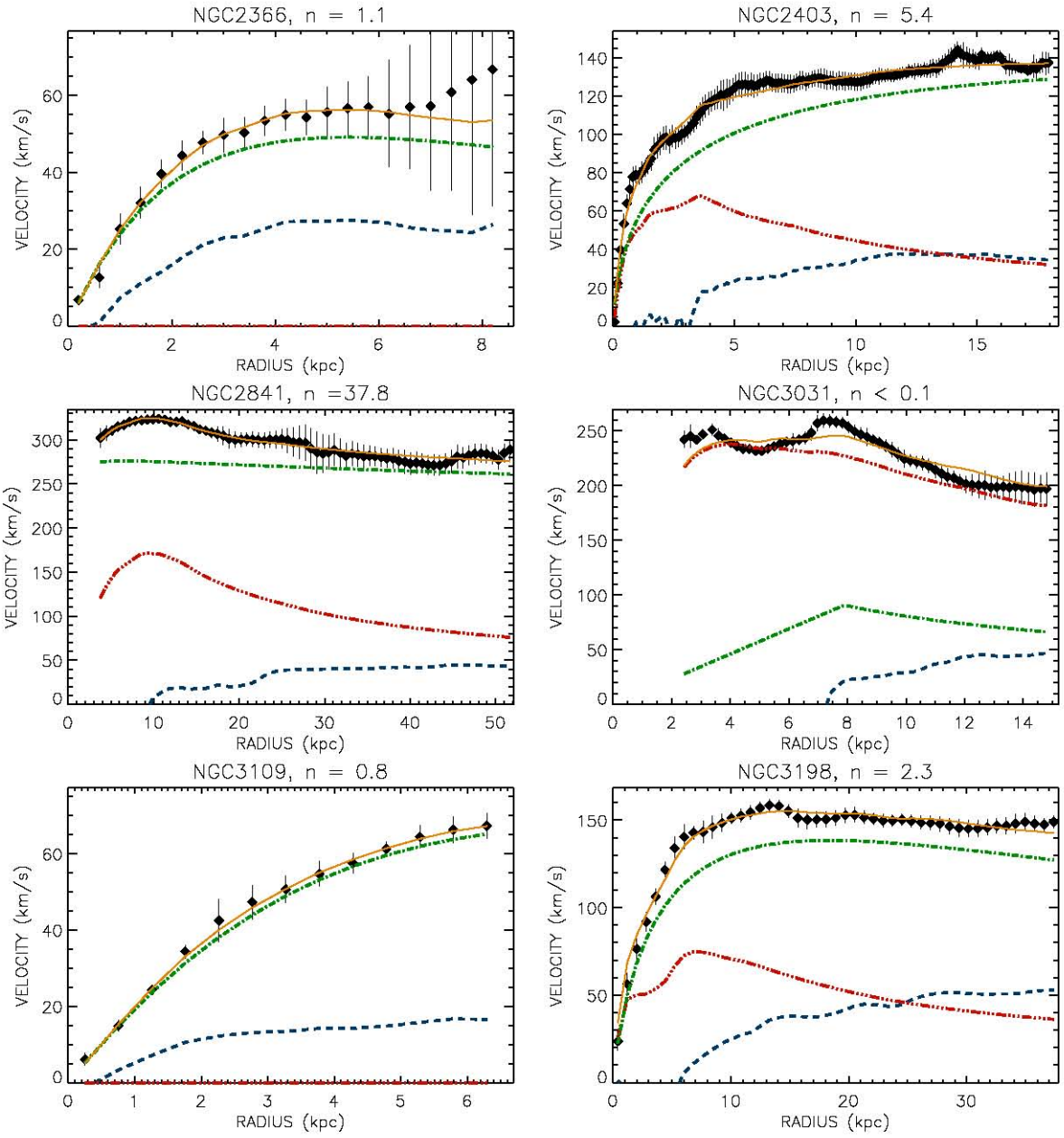

Figure 22: Mass model results using Einasto DM halo model with M/L free (continued)

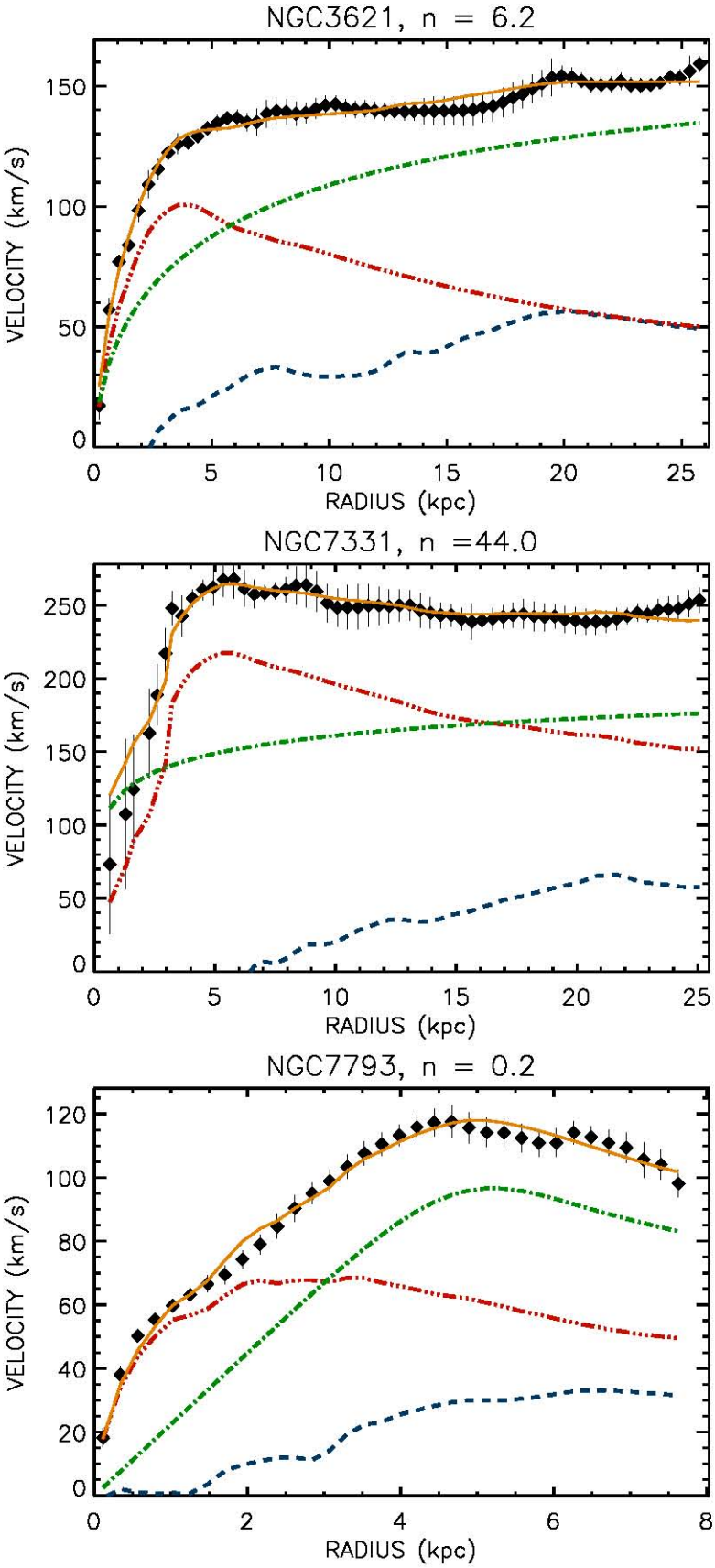

Figure 23: Mass model results using Einasto DM halo model with M/L free (continued)

Table 5: Mass model results for the Einasto dark matter halo model, M/L fixed (Kroupa IMF).

Name	χ^2_r	ρ_{-2} $M_\odot$ pc^{-3}	r_{-2} kpc	n
1	2	3	4	5
DDO154	0.29	1.4 ± 0.3	5.9 ± 0.8	2.2 ± 0.3
IC2574	0.23	0.7 ± 0.4	15.8 ± 6.9	0.9 ± 0.4
NGC55	0.73	2.5 ± 0.4	8.9 ± 0.3	0.2 ± 0.1
NGC247	1.29	0.8 ± 0.8	10.8 ± 6.2	1.9 ± 0.9
NGC300	0.75	7.3 ± 0.7	4.8 ±0.2	2.2 ± 0.3
NGC925	1.07	3.4 ± 9088.0	10.1 ± 58400.0	0.1 ± 1320.3
NGC2366	0.21	5.4 ± 1.1	3.2 ±0.3	1.1± 0.2
NGC2403	0.55	1.5 ± 0.3	15.6 ± 2.0	5.6 ± 0.5
NGC2841	3.39	1.6± 0.4	30.2 ± 3.5	0.7± 0.2
NGC3031	2.79	10.2 ± 5.7	7.5 ± 7.5	0.1 ± 0.3
NGC3109	0.26	4.9 ± 0.9	5.0 ±0.6	0.6± 0.1
NGC3198	0.81	2.2 ± 0.2	13.1 ± 0.6	2.1 ± 0.3
NGC3621	0.70	0.6 ± 0.2	27.2 ± 6.6	2.6 ± 0.5
NGC7331	0.43	0.1 ± 0.2	6270.0 ± 279000.0	3.8 ± 27.9
NGC7793	1.65	22.7 ± 1.9	3.7 ± 0.1	0.34 ± 0.1
	<1.01 >			

col. 1: Galaxy name
col. 2: reduced chi-squared
col. 3: local density at r_{-2}
col. 4: Radius where the density profile has a slope of -2
col. 5: Einasto index

Table 6: Mass model results for the Einasto dark matter halo model with M/L free.

Name	χ^2_r	ρ_{-2} $M_\odot$ pc^{-3}	r_{-2} kpc	n	M/L
1	2	3	4	5	6
DDO154	0.28	1.7 ± 0.4	5.5±0.6	0.8±0.3	2.6
IC2574	0.2	0.8 ± 0.2	13.1 ± 2.3	1.3 ± 0.2	0.0
NGC55	0.19	3.7 ± 0.2	6.8 ± 0.2	1.1 ± 0.1	0.0
NGC247	1.34	0.9± 0.9	10.7 ± 12.7	2.12 ± 4.6	0.9
NGC300	0.70	9.4 ± 0.7	4.4 ± 0.2	2.29 ± 0.3	0.0
NGC925	0.41	4.9 ± 0.3	8.3 ± 0.2	0.12 ± 0.1	0.2
NGC2366	0.17	6.2 ± 1.2	3.1 ± 0.3	1.13 ± 0.2	0.0
NGC2403	0.56	1.4 ± 0.4	16.4 ± 2.5	5.42 ± 0.6	0.3
NGC2841	0.17	223.4 ± 128.2	2.5 ± 0.7	37.7 ± 16.6	0.3
NGC3031	2.73	7.2 ± 5.1	7.7 ± 10.6	0.1 ± 0.3	0.5
NGC3109	0.20	4.5 ± 0.8	5.1 ± 0.6	0.8 ± 0.1	0.0
NGC3198	0.69	4.8 ± 1.2	9.5 ± 0.9	2.2± 0.2	0.3
NGC3621	0.56	0.2 ± 0.1	42.8 ± 14.5	6.2 ± 1.2	0.3
NGC7331	0.35	540.0± 0.1	669.0 ± 9100.0	44.0 ± 112.5	0.3
NGC7793	0.81	20.6 ± 1.4	4.1 ± 0.1	0.1 ± 0.1	0.2
	<0.62 >				

col. 1: Galaxy name
col. 2: reduced chi-squared
col. 3: local density at r_{-2}
col. 4: Radius where the density profile has a slope of -2
col. 5: Einasto index
col. 6: Mass-to-light ratio

4.3 Discussion

MOND with one parameter fits (a_0 fixed) also known as MOND fits are shown on the left panels of Figure 8 to 12. The MOND fits are remarkably good for NGC 3621 and NGC 7331. These two galaxies are bright spirals which are dominated by normal circular motions (de Blok et al. 2008).

Discrepancies between the rotation curves predicted by MOND and the observed rotation curves are seen for the remaining galaxies. The difference between the MOND fits and the observed rotation curves is less significant for the following galaxies: NGC 0055, NGC 0247, NGC 2366, NGC 3031 and NGC 2848. This is justified by their reduced χ^2 listed in Table 3. However, disagreement between the rotation curves predicted by MOND and the observed rotation curves are clearly noticed for the following galaxies NGC 925, NGC 2403, NGC 3109, NGC 3198 and NGC 7793 in which MOND overestimates the rotation velocities in the inner region of the galaxy and underestimates them in the outer parts.

The quality of the fits is largely improved when the MOND acceleration constant a_0 is taken as a free parameter for all the galaxies in our sample with the exception of NGC 3109. MOND fits with two free parameters (M/L, a_0) are shown on the right panels of Figure 8 to 12.

The best fits are obtained using the Einasto dark matter halo models. The average reduced chi-square for Einasto models (both M/L fixed $< \chi_r^2 > = 1.01$ and M/L free $< \chi_r^2 > = 0.62$) are lower compared to the ISO halo ($< \chi_r^2 > = 1.94$), NFW halo ($< \chi_r^2 > = 2.16$) and MOND with a_0 free ($< \chi_r^2 > = 2.47$).

4.3.1 Models with Distance Free and a_0 Fixed

In order to check the effect of the uncentainties on the distance. We performed MOND fits for NGC 3109 and NGC 3198 by letting the distance vary within the uncertainties listed in table 1. The results are shown in figure 24 for NGC 3198, and in figure 25 for NGC 3109.

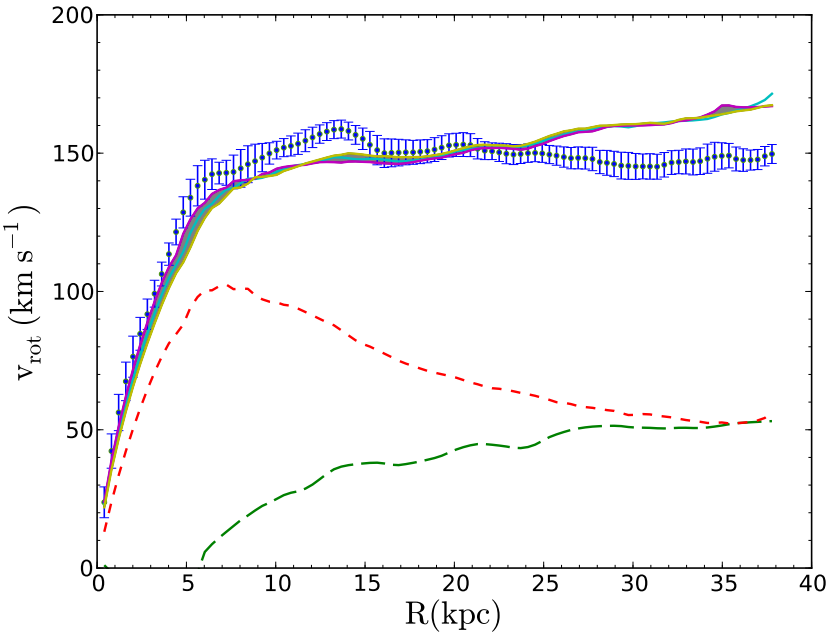

Figure 24: MOND fit result for NGC 3198 with distance free within the error-bars, a_0 was fixed to its standard value. The shaded area shows the best MOND fit results.

The quality of the MOND fits for NGC 3198 is slightly improved when the distance is smaller than the ceipheid distance and even worse if the distance is larger (D = 12.85 Mpc, χ^2_{red} = 5.62; D = 13.80 Mpc, χ^2_{red} = 5.68; D = 14.75, χ^2_{red} = 6.21). An acceptable MOND fit could only be obtained for NGC 3198 if the distance is much smaller compared to the ceipheid distance of 13.80 Mpc (Begeman et al. 1991; Bottema et al. 2002). For NGC 3109, the error-bar on the distance has no effect on the quality of the MOND fit, since the uncertainty on the ceipheid distance is quiet small (less than 10 percent) for this galaxy. These results show that uncertainties on

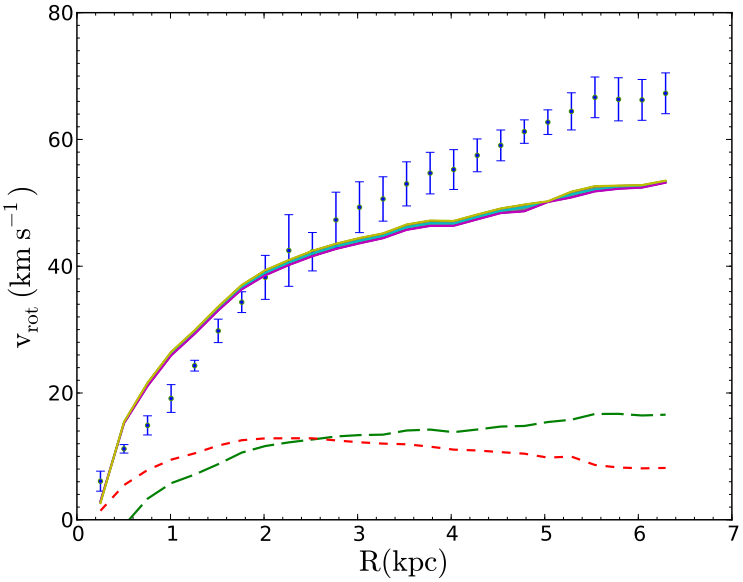

Figure 25: MOND fit result for NGC 3109 with distance free within the error-bars, a_0 was fixed to its standard value. The shaded area shows the best MOND fit results.

the distance have very small impact on the MOND fits result when ceipheid-based distances are used.

4.3.2 DDO 154: Gas Rich Dwarf Galaxy

DDO 154 is a gas rich dwarf galaxy which has been studied extensively in the context of MOND. Milgrom & Braun (1988) named DDO 154 as an acute test of MOND because of its internal acceleration deeply in the MOND regime which is characterised by the acceleration threshold value a_0. The poor MOND fit for DDO 154 has been interpreted to be due to the uncertainties on the measured distance since no measured cepheid based distance is available for this galaxy. The adopted distance for DDO 154 in this work was determined using the brightest stars by Karachentsev et al. (2004). The uncertainties of the inclination is also known to be one of the source of the poor quality MOND fit for DDO 154 due to the unknown thickness of the HI disk.

Recently, Angus et al. (2012) used a new N-body code which solves the modified Poisson's equation and fits galaxy rotation curves. They performed a four parameters (M/L, stellar & gas disk scale heights and distance) MOND fits for five galaxies from THINGS. They found that an acceptable MOND fit could be obtained for DDO 154 when the gas disk scale height is taken as $z_g = 1.5$ and with higher M/L.

4.3.3 IC 2574 and NGC 925: Galaxies Dominated by non-Circular Motions

Gentile et al. (2011) mentioned the presence of holes and shells in the HI gas distribution of these two galaxies. The existence of large non-circular motions has also been noticed by Oh et al. (2008). However, the fits results for the ISO and Einasto are remarkably good with a reduced chi-square of 1.22 and 0.2 respectively for IC 2574 and 2.09 and 1.07 for NGC 925. MOND produces poor fits for these two galaxies even if a_0 was taken as free parameter. The poor MOND fits for IC 2574 and NGC 925 can not be due only to the presence of non-circular motions since the dark matter (ISO and Einasto) fits are reasonably good. The mass model for IC 2574 with the ISO halo is shown on the left of the middle panel of figure 13. The stellar contribution is much higher compared to the MOND fits with one and two free parameters as shown in the middle panel of figure 8. For NGC 925, the Einasto halo model provides a good fit to the rotation curves as shown in figure 18 compared to MOND in figure 8, ISO and NFW halo fits in figure 14.

4.3.4 NGC 3109: A Nearby Magellanic Type Spiral Galaxy

As shown on the middle panel of figure 11, NGC 3109 has the largest discrepancies between the predicted MOND rotation curves and the observed rotation curves. The highest difference goes up to 10 km/s on the outer part of the rotation curves. This disagreement between the MOND rotation curves and the observed rotation curves

remained even when a_0 was taken as a free parameter. However, the derived M/L of the stellar disk remain constant for both MOND fit (a_0 fixed) and MOND with two free parameter fit (M/L and a_0). Begeman et al. (1991) pointed out that not all the HI gas content of the galaxy is detected and therefore, the gas contribution need to be increased by a factor of 1.67 to take into account this undetected HI gas. However, Jobin & Carignan (1990) measured a total HI mass of 2.9 x 10^8 $M_\odot$ from VLA observations (hydrib VLA C-D configuration) using the distance of 1.3 Mpc. This is smaller compare to the result found by Barnes & de Blok (2001) using HIPASS observations (Multibeam data with the Parkes 64m dish) of 4 $\times$ 10^8 $M_\odot$. This difference could be due to some missing fluxes for the VLA data because of the lack of sensitivity. Therefore, new HI observations using the Karoo Array Telescope (KAT 7) (SKA and MeerKAT precursor) and the Karl Jansky Very Large Array (JVLA) for NGC 3109 will be used to confirm these findings, which is therefore part of our future work. NGC 3109 is problematic for MOND, but more analysis needs to be done. For example, more accurate information is required for the stellar and gas disk scale lengths and detailed analysis of the velocity field is needed to quantify the effect of an eventual interaction between NGC 3109 and the Antila dwarf.

4.3.5 NGC 3198: A Bright Spiral Galaxy

NGC 3198 is another galaxy for which an acceptable MOND fit could not be obtained. One and two free parameters MOND fits for this galaxy is shown in the bottom panel of figure 11. It has been reported in the literature that MOND fits require lower distances than the measured cepheid distance of 13.80 Mpc. However, Bottema et al. (2002) found that a good MOND fit to the rotation curves could be made using the cepheid distance with a lower a_0 (0.9×10^{-8} cm s^{-2}).

4.3.6 Correlation Between the MOND Acceleration Constant a_0 and other Galaxy Parameters

Any systematic trend of a_0 with some galaxy parameter could be a problem for MOND since it is an universal constant. We investigated the possibility of a correlation between the corrected central surface brightness and disk scale length with the MOND parameter a_0. As shown in figure 26, we found that galaxies with larger disk scale length and higher central surface brightness required higher values of a_0 and galaxies with smaller disk scale length and lower central surface brightness a lower a_0 values. This also has been seen in the R-band for LSB galaxies by Swaters et al. (2010). Gentile et al. (2011) did the same analysis using the 3.6 microns band for twelve (12) galaxies from the THINGS sample and found no correlation. However, the bulge central surface brightness were used for their study instead of the disk values.

Plot of a_0 versus the B-band extrapolated central surface brightness is shown on top panel of figure 26 and the correlation between a_0 and the optical disk scale length is shown on bottom panel, the same correlations are shown in figure 27 for the 3.6 microns bands. This plot shows that, there is a correlation between a_0 and these two parameters. These correlations contradict the fact that the MOND acceleration a_0 is a constant and should not depends on any galaxies parameters. We found the following correlations in the B-band :

$$a_0 = (-0.78 \pm 0.41) \times B(0)_c + (22.71 \pm 0.57 \qquad \chi_r^2 = 1.23 \qquad (33)$$

$$a_0 = (0.28 \pm 0.19) \times \alpha^{-1} + (1.64 \pm 0.26) \qquad \chi_r^2 = 0.25 \qquad (34)$$

and the following correlations in the 3.6 micron band :

$$a_0 = (-0.15 \pm 0.13) \times \mu_{3.6}(0)_c + (4.04 \pm 2.54) \qquad \chi_r^2 = 0.63 \qquad (35)$$

$$a_0 = (0.38 \pm 0.43) \times \alpha_{3.6}^{-1} + (3.15 \pm 0.60) \qquad \chi_r^2 = 1.34 \qquad (36)$$

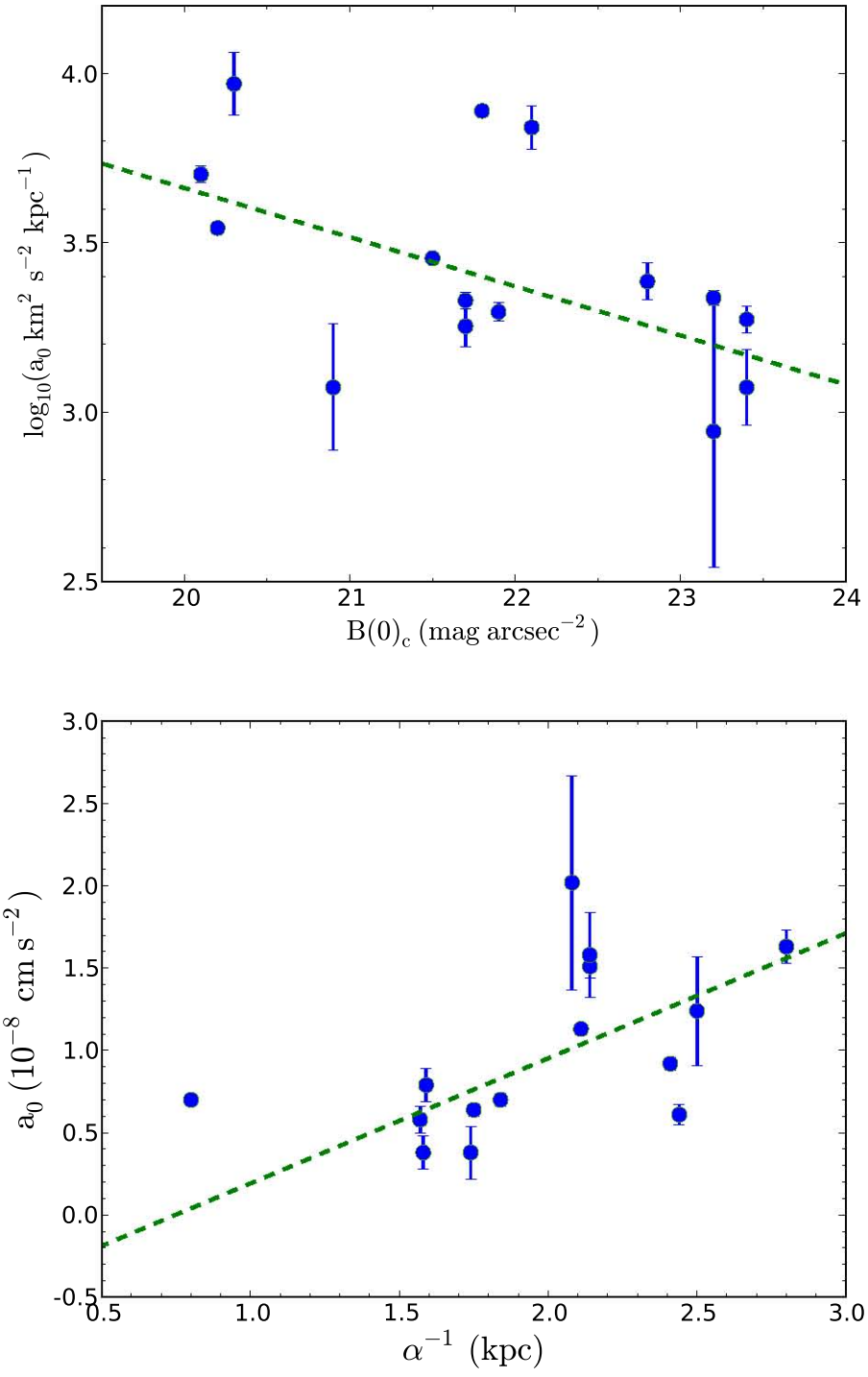

Figure 26: Top panel: MOND parameter a_0 as a function of the extrapolated B-band corrected disk central surface brightness. Bottom panel: MOND parameter a_0 as a function of the disk scale length in kpc. The best fits are shown as dashed lines.

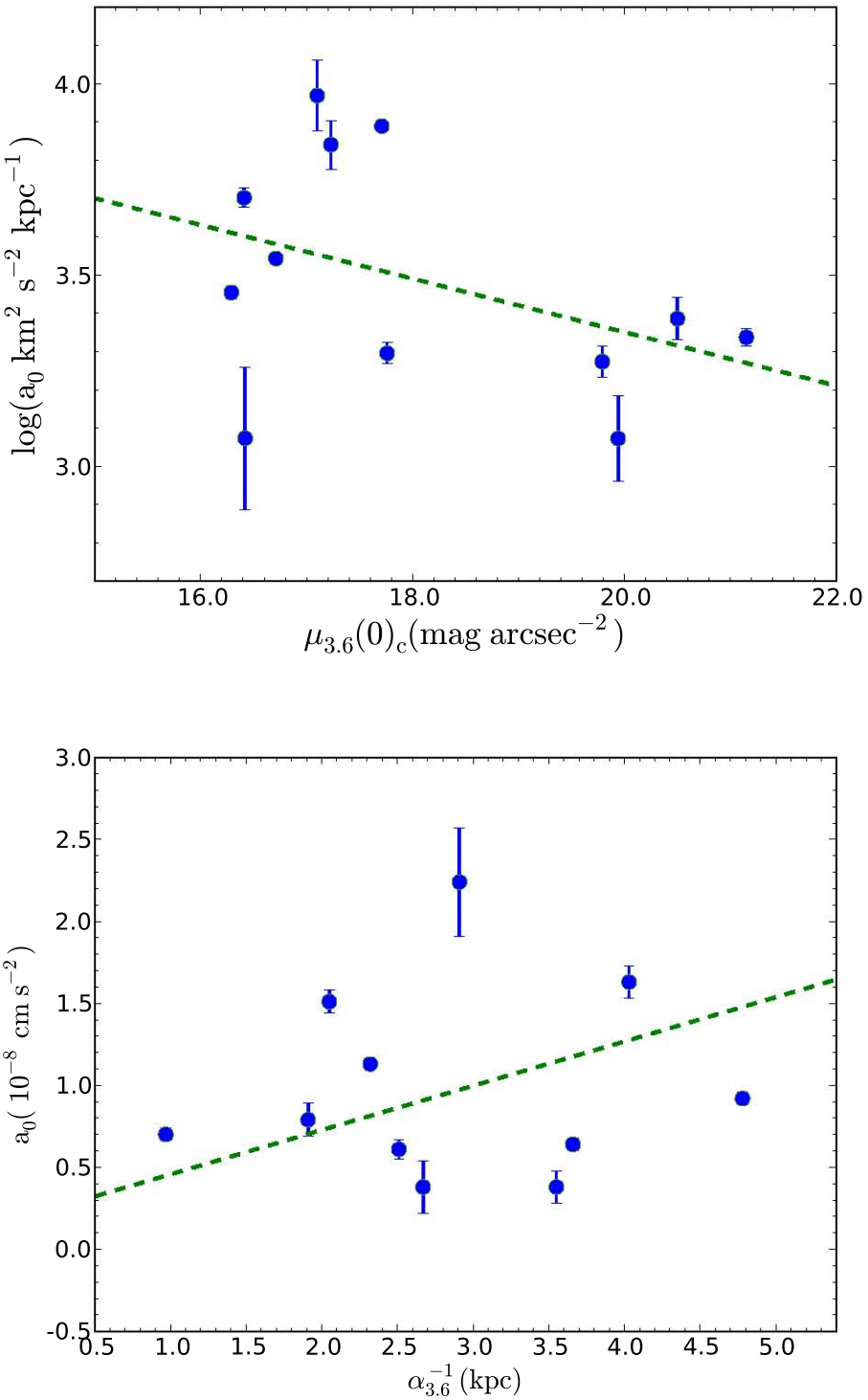

Figure 27: Top panel: MOND parameter a_0 as a function of the extrapolated 3.6 micron band corrected disk central surface brightness. Bottom panel: MOND parameter a_0 as a function of the disk scale length in kpc. The best fits are shown as dashed lines.

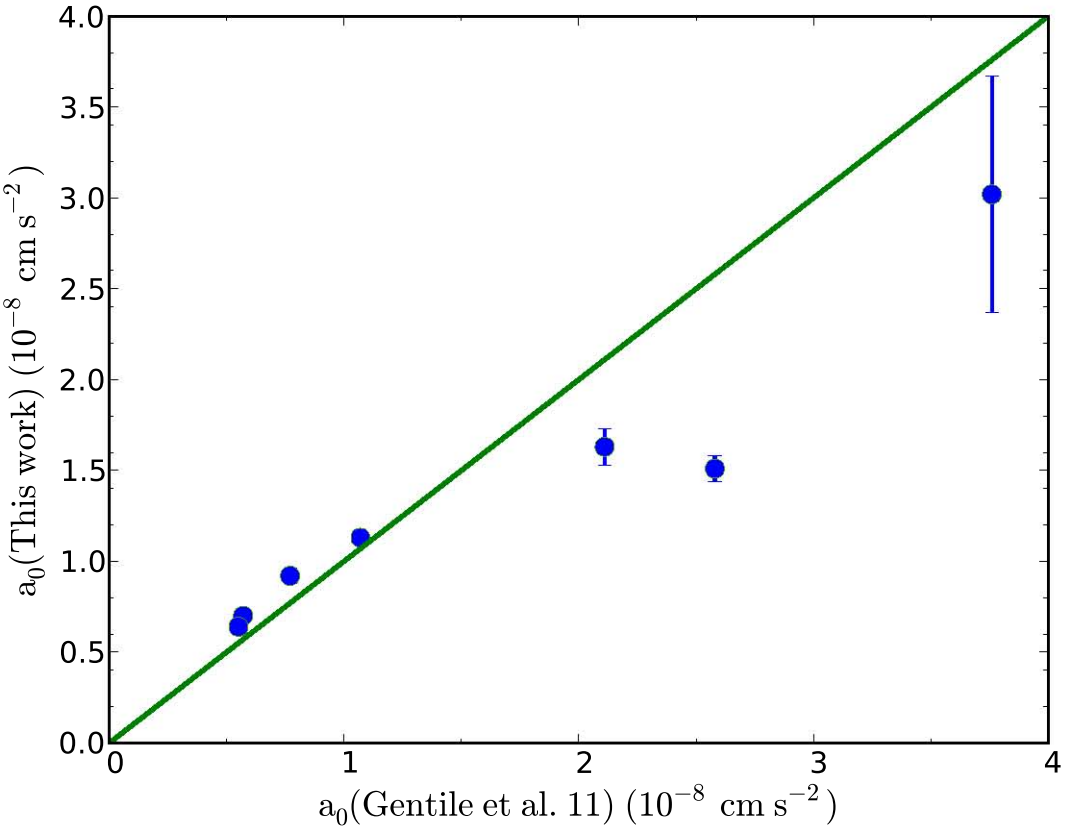

Figure 28: Comparison between a_0 derived in this work and Gentile et al. (2011)

We also found large scatter between the maximum and minimum value for a_0 found in this work. We compared a_{0max} and a_{0min} with the standard value of the acceleration parameter $a_0 = 1.21 \times 10^{-8}$ cm s^{-2}. We found the following results:

$$a_{0max} - a_0 = ((3.02 \pm 0.65) - 1.21) \times 10^{-8} cm\ s^{-2} \ = \ (1.81 \pm 0.65) \ \times 10^{-8} cm\ s^{-2}$$

$$a_0 - a_{0min} = (1.21 - (0.38 \pm 0.16)) \times 10^{-8} cm\ s^{-2} \ = \ (0.83 \pm 0.16) \ \times 10^{-8} cm\ s^{-2}$$

These results need to be confirmed with larger samples because it contradicts the fact that galaxies with low central surface brightness which are in the MOND regime are more likely to have higher a_0 than galaxies with high central surface brightness. We compared our estimated a_0 with those calculated by Gentile et al. (2011) and found no significant departure. The comparison between a_0 derived in this work and Gentile et al. (2011) is shown in figure 28, our estimated parameters are much lowers than those estimated by Gentile et al. (2011) for three galaxies out of seven.

4.3.7 Dark Matter Halo Scaling Laws

The common ways to explain the flatness of galaxies' rotation curves is by adding dark matter halo to the visible matter (gas and stars). The halo is characterised by a theoretical density profile. It has been known that the observational motivated ISO halo provides a better description of the observed rotation curves as compared to the cosmological motivated NFW halo (see e.g. de Blok et al. 2001). The success of the ISO halo for fitting galaxies rotation curves has been criticised to be due to the number of parameters involve in the fitting procedures. These parameters are the halo core radius R_C and the halo central density ρ_0. Therefore, the correlation between these two parameters have been investigated in the literature (Kormendy & Freeman 2004; Barnes et al. 2004; Spano et al. 2008). These studies aim to minimise the numbers of free parameters involved in the ISO halo mass model. The relationship between R_C and ρ_0 is found by plotting the core radius (log) against the central density (log) of the halo .

The correlation found by Kormendy & Freeman (2004) is:

$$log\ \rho_0 = -1.04 \times log\ R_C - 1.02 \tag{37}$$

And the result by Spano et al. (2008) was

$$log\ \rho_0 = -0.93 \times log\ R_C - 0.74 \tag{38}$$

A similar analysis was undertaken for our sample galaxies to look for this correlation which is shown in Figure 29. A plot of the core radius as a function of the central densities is shown on the top panel of 29. The filled blue points show the results of the ISO model with M/L free, the open circle are for the ISO model results with M/L fixed (Kroupa IMF) and the open squares are for the ISO model result with M/L fixed (Diet-Salpeter IMF).We found that our result is consistent with those presented in the literature. This confirms the existence of a scaling relation for the central core of the dark matter halos.

The following relationship was found using a simple least square method:

$$log\ \rho_0 = -1.10 \times log\ R_C - 1.08 \tag{39}$$

The correlation between the characteristic radius and the characteristic density of the Einasto halo is shown on the bottom panel of figure 29. The correlation found in this work is:

$$log\ \rho_{-2} = -1.90 \times log\ r_{-2} + 2.36 \tag{40}$$

Result found by Chemin et al. (2011) is:

$$log\ \rho_{-2} = -2.25 \times log\ r_{-2} + 0.20 \tag{41}$$

The core radius (logarithm) is plotted as a function of absolute magnitude in Figure 30. Clear correlation is seen between these two parameters, low-luminosity galaxies correspond to a small core radius.

As shown in figure 30 our least square fit results are :

$$log\ \rho_0 = 0.123 \times M_B + 0.41 \tag{42}$$

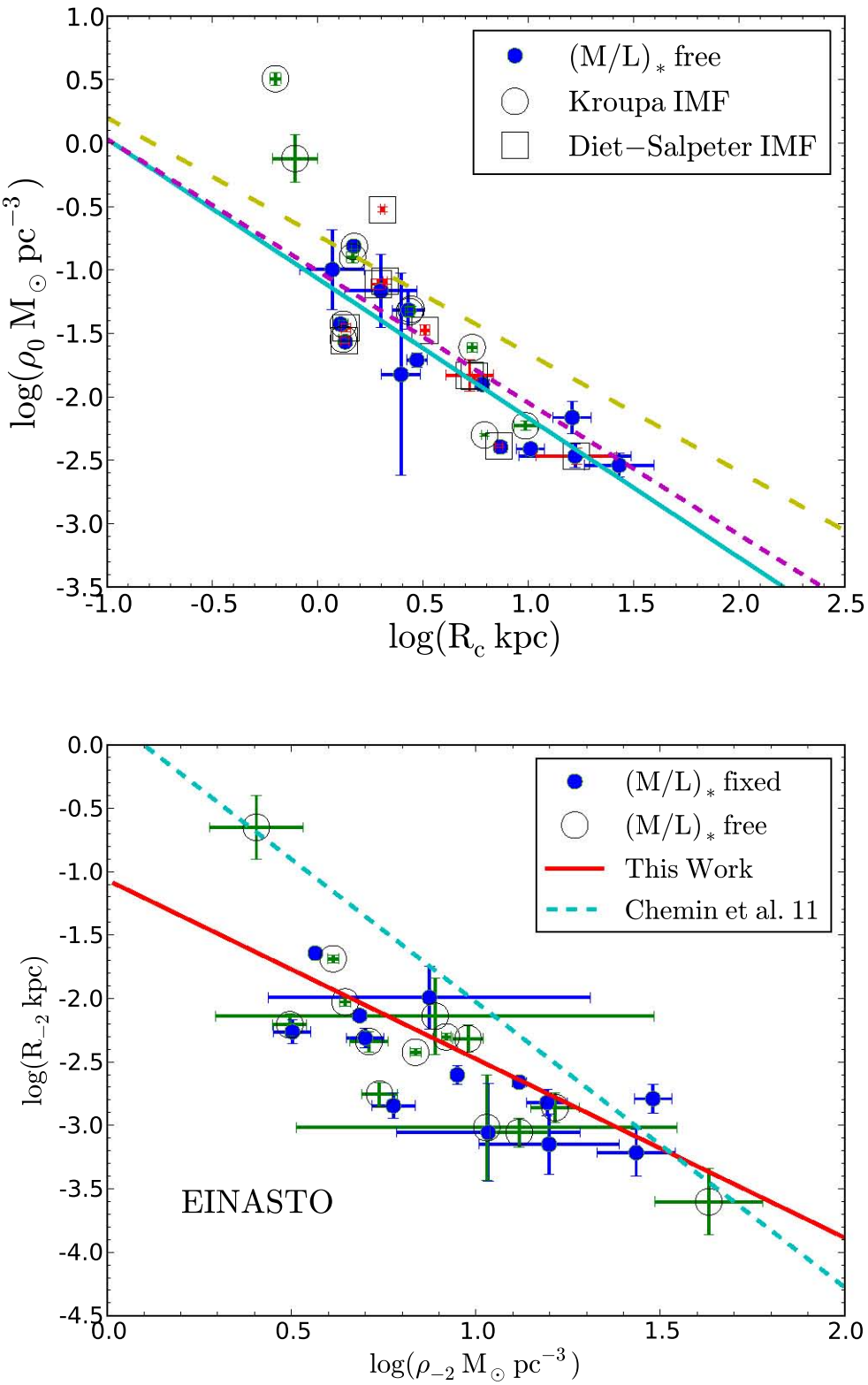

Figure 29: Top panel: Core radius (log)vs central density (log) for ISO halo. The bold green line shows the best fit result found in this study, the long dashed yellow lines is the correlation found by Spano et al. (2008) and the red dashed lines is the correlation found by Kormendy & Freeman (2004) . Bottom panel: central density (log) of the halo as a function of central density (log) for Einasto halo. Lines and symbols are described on the graph.

$$log\ r_c = -0.132 \times M_B - 1.76 \tag{43}$$

The least square result found by Spano et al. (2008) were:

$$log\ \rho_0 = 0.142 \times M_B + 1.29 \tag{44}$$

$$log\ r_c = -0.167 \times M_B - 2.47 \tag{45}$$

And the results by Kormendy & Freeman (2004) were:

$$log\ \rho_0 = 0.113 \times M_B + 0.12 \tag{46}$$

$$log\ r_c = -0.127 \times M_B - 1.42 \tag{47}$$

The correlation between the central density and the absolute magnitude was also investigated which is shown in bottom panel of figure 30. We found that the least square fit found results by Kormendy & Freeman (2004) and those found in this work are in good agreement.

Kormendy & Freeman (2004) investigated the correlation between the surface density of the halo and galaxy luminosity, they found that the halo surface density is constant, independently of morphology type and absolute magnitude. The halo surface density is given by the product of the core radius of the halo and the central density of the halo. They found that the surface density of the halo is nearly constant as a function of absolute magnitude. This result was confirmed by Spano et al. (2008) which is shown as red dashed line in figure 31. We found a correlation which is consistent with those found in the literature.

Kormendy & Freeman (2004):

$$\rho_0\ R_C \sim 100\ M_\odot\ pc^{-2} \tag{48}$$

Spano et al. (2008):

$$\rho_0\ R_C \sim 150\ M_\odot\ pc^{-2} \tag{49}$$

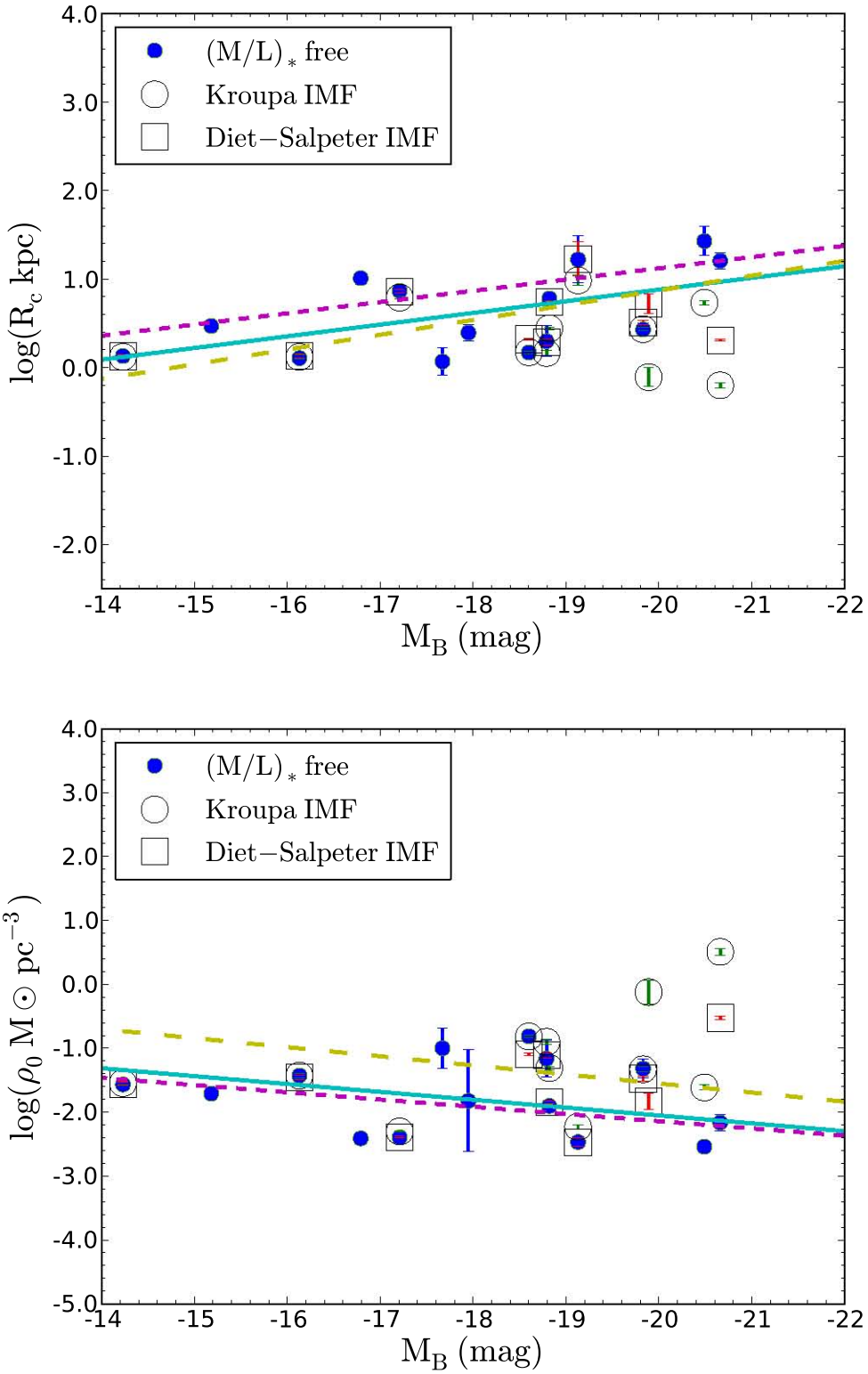

Figure 30: Top panel: Core radius (log) of the halo (ISO model) as a function of absolute magnitude. Bottom panel: central density (log) of the halo as a function of absolute magnitude (ISO model). The bold green line shows the correlation found in this study, the long-dashed yellow line is the correlation found by Spano et al. (2008) and the dashed red line is the correlation found by Kormendy & Freeman (2004).

This work:

$$\rho_0 \; R_C \sim 120 \; M_\odot \; pc^{-2} \tag{50}$$

The difference seen in the figure 31 between the correlation found by Spano et al. (2008) and this work is due to the fact that Spano et al. (2008) used an Isothermal sphere while a pseudo-Isothermal sphere is used in this work. The main difference between these two model is the definition of the core radius. However, the slopes are in good agreement. This correlation implies that the dark matter ISO halo could be characterised by only one parameter since the core radius and the central density of the halo are correlated. These results also confirm the scaling laws for dark matter halos, which is important for the understanding of the relation between the dark and luminous matter and the characteristics of the dark matter itself. This also implies that low luminosity galaxies have smaller core radius and higher central densities.

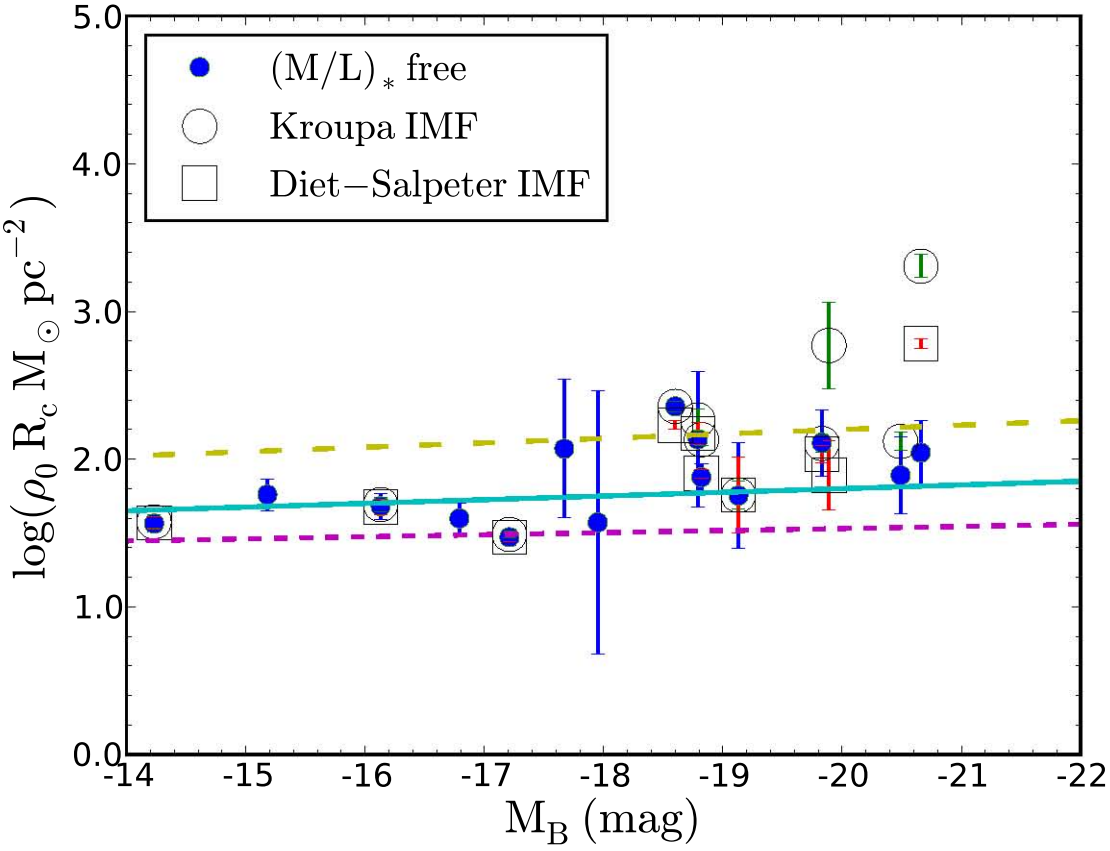

Figure 31: Plot of the central surface densities of the DM halo (ISO) as a function of absolute magnitude. The green line shows the correlation between found in this study, the long-dashed yellow line is the correlation found by Spano et al. (2008) and the dashed red line is the correlation found by Kormendy & Freeman (2004).

4.3.8 Resampled Rotation Curves

The effect of the sampling of the rotation curves was checked by comparing the parameters estimated by de Blok et al. (2008) for the dark matter ISO halo model (M/L free) and this work for eleven galaxies. The rotation curves of the THINGS were oversampled with two points per beam size. Therefore a resampled version of the THINGS rotation curves with one point per beam were used as suggested by Chemin et al. (2011). This is important in term of homogeneity of the rotation curves of our sample galaxies and to ensure that all points are independant. Comparison between the core radius and the central density of the halo from de Blok et al. (2008) and this work are shown on Figure 32. We found larger value for the core radius compared to de Blok et al. (2008) and lower values for the central densities. This could be due to the number of points on the rotation curves used for the mass models. This difference is largely noticed for NGC 2841, NGC 7331 and NGC 925. However, our reduced chi-squared listed in Table 4 are higher compared to their values obtained using the THINGS rotation curves, which is to be expected due to the oversampling of their rotation curves.

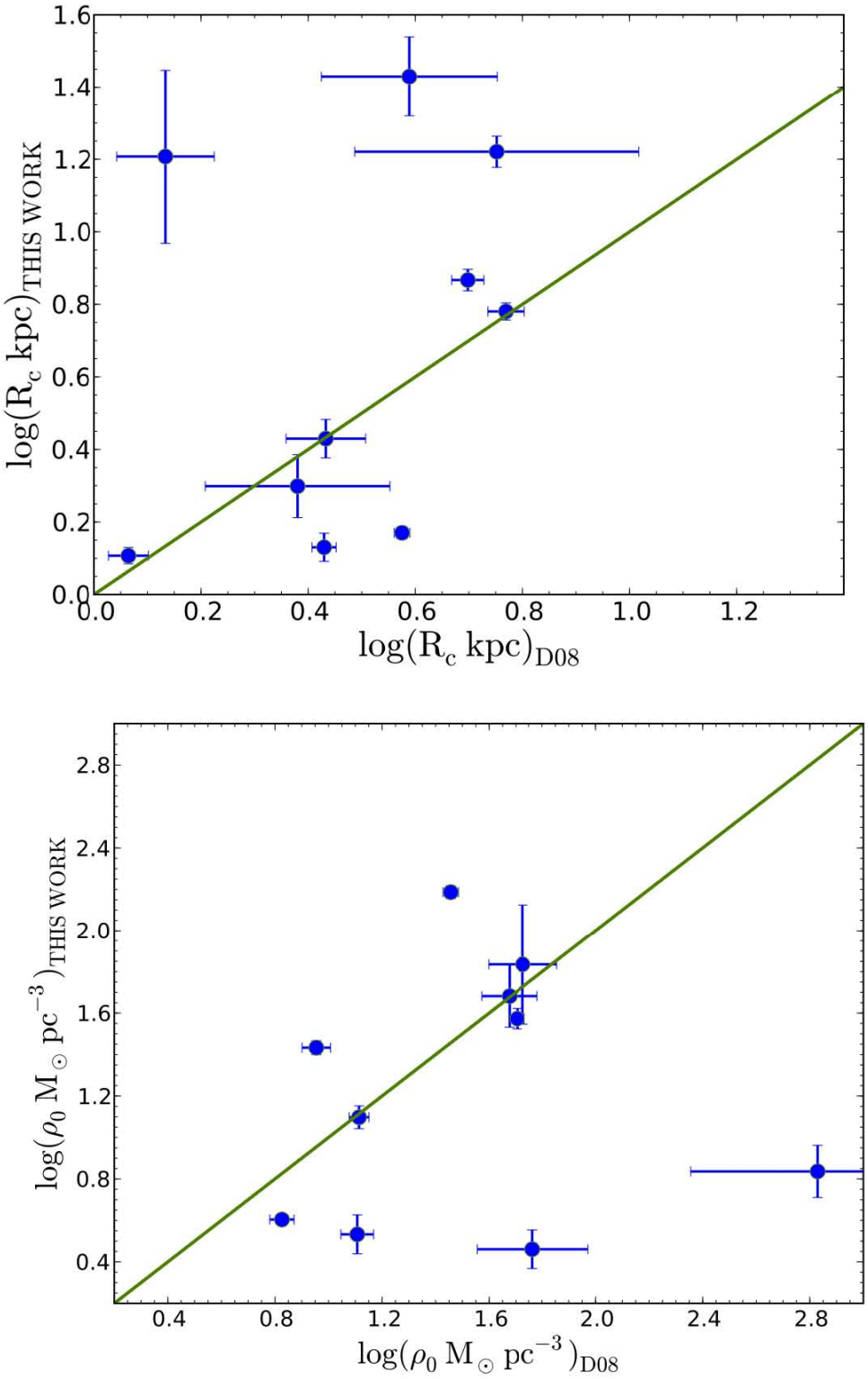

Figure 32: Comparison between the core radius and the central density of the ISO halo from de Blok et al. (2008) and this work. Top panel: Core radius (log) of the halo from de Blok et al. (2008) vs Core radius (log) of the halo from this work. Bottom panel: central density (log) of the halo from de Blok et al. (2008) vs central density (log) of the halo from this work. The M/L was taken as a free parameter.

Chapter 5

Conclusions & Future Work

5.1 Conclusions

We have presented mass models for fifteen (15) dwarf and spiral galaxies selected from the literature. Their observed rotation curves were confronted with Milgrom's MOdified Newtonian Dynamics (MOND), the observationally motivated ISO dark matter halo model, the cosmologically motivated NFW halo model and the Einasto dark matter halo model. The galaxies in the sample were selected to be homogenous in term of their measured distances, the sampling of their rotation curves and the availability of the 3.6 microns band used to estimate the stellar contribution. The selected galaxies in the sample cover a large range of luminosities and morphological types.

The models were carried out using the GIPSY software tasks ROTMOD and ROTMAS and the results were analysed using the programming language PYTHON.

MOND with one free parameter (M/L) and two free parameters (M/L, a_0) were performed. MOND fits with a_0 free were needed to re-estimate the average value of a_0, to identify galaxies in which a_0 exhibits a significant departure from the standard value of $a_0 = 1.21 \times 10^{-8}$ cm s^{-2} and to look for any trend between a_0 and the other parameters of the galaxy.

The MOND fit results are:

- An average value of $(1.01 \pm 0.10) \times 10^{-8}$ cm s^{-2} was measured for the MOND acceleration constant a_0 which is smaller compared to the standard value of 1.21×10^{-8} cm s^{-2} found by Begeman et al. (1991) and should be considered as the standard value since our sample covers a broader range of luminosities and morphological types.

- The rotation curves predicted by MOND are only in good agreement with the observed rotation curves for bright spirals with normal circular motions.

- The difference between the rotation curves predicted by MOND and the observed rotation curves is the largest for NGC 3109. This was seen for MOND with one free parameter fits (M/L) and MOND with two free parameters fits (M/L and a_0). Therefore, no MOND model can fit the data for NGC 3109.

- Correlation between a_0 and the extrapolated central surface brightness and disk scale length were found. We found that galaxies with larger disk scale length and higher surface brightness require higher values of a_0 and galaxies with small disk scale length and lower surface brightness prefer lower a_0. This is a great problem for MOND.

We found that the Einasto halo model provides much better fits to the rotation curves compared to the other models from the overall results. This was seen for the model with M/L fixed and M/L free. The fits are remarkably good for M/L free, however the Einasto halo model with M/L free preferred $\mathbf{M/L = 0}$ for more than half of the galaxies in the sample which is unphysical. The reduced qui-squared for the Einasto halo with M/L fixed ($< \chi^2_r > = 1.01$) is still smaller compare to the ISO halo ($< \chi^2_r > = 1.94$), the NFW halo ($< \chi^2_r > = 2.16$) and MOND with a_0 free ($< \chi^2_r > = 2.47$). However, the unphysical stellar disks obtained with the Einasto models suggests that the goodness of the fit is not sufficient to favour this model over the others. This is why, considering the more realistic stellar disks obtained

with the ISO halo models, we can say that it produces the best representation of the observed rotation curves.

The existence of the scaling relations for the central core of the dark matter halos were investigated for the ISO and Einasto halo models. Correlation between the central density ρ_0 and the core radius R_c were found. This correlation implies that the central dark matter halo could be characterised by one of the two parameters since they are correlated. We also found that low-luminosity galaxies tend to have smaller core radii and higher central densities. It has been presented in the literature that the halo surface density is almost constant. This was also found in our sample galaxies for the ISO halo, this correlation is similar to the fundamental plane for elliptical galaxies. We found $\rho_0\ R_C \sim 120\ M_\odot\ pc^{-2}$ which is in good agreement with previous studies: such as Kormendy & Freeman (2004) ($\rho_0\ R_C \sim 100\ M_\odot\ pc^{-2}$) and Spano el al. (2008) ($\rho_0\ R_C \sim 150\ M_\odot\ pc^{-2}$). This implies that the central core of the dark matter halo could be defined by only one parameter, therefore the number of free parameters of the mass model using ISO dark matter halo is reduced to one when M/L is fixed.

These findings need to be confirmed with a larger sample. More analysis of the rotation curves is also needed to enhanced the accuracy of the parameters obtained for the mass models. For instance the effect of bars and warps have to be taken into account. More than half of the galaxies in the sample have bar structures and the effect of the gas streaming along the bars could have an effect of the rotation velocities of the galaxy in the inner parts. The M/L used to convert the stellar disk surface brightness profile into mass density also is an important parameter for the mass model. It has been claimed that M/L should be three times lower than those obtained from the stellar synthesis model (Bershady et al. 2011). This could lead to different results from those obtained in this work and could not be neglected.

5.2 Future Work

As a future work, 3.6 microns IRAC surface brightness profiles will be used for all the galaxies in the sample for the stellar disk contributions. New VLA data (when available) will be retrieved from the archive for the galaxies which are not part of THINGS to derive their rotation curves. For NGC 3109, HI observations using the Karoo Array Telescope (KAT 7) (SKA and MeerKAT precursor), the Karl Jansky Very Large Array (JVLA) and the GBT single dish will be used.

Bibliography

Angus G. W., van der Heyden K. J., Famaey B., Gentile G., McGaugh S. S., de Blok W. J. G., 2012, MNRAS, 421, 2598

Barnes D. G., de Blok W. J. G., 2001, AJ, 122, 825

Barnes E. I., Sellwood J. A., Kosowsky A., 2004, AJ, 128, 2724

Begeman K. G., 1989, A&A, 223, 47

Begeman K. G., Broeils A. H., Sanders R. H., 1991, MNRAS, 249, 523

Bershady M. A., Martinsson T. P. K., Verheijen M. A. W., Westfall K. B., Andersen D. R., Swaters R. A., 2011, ApJL, 739, L47

Bosma A., 1978, PhD thesis, PhD Thesis, Groningen Univ., (1978)

Bottema R., Pestaña J. L. G., Rothberg B., Sanders R. H., 2002, A&A, 393, 453

Bournaud F., Combes F., 2004, in Astrophysics and Space Science Library, Vol. 319, Penetrating Bars Through Masks of Cosmic Dust, Block D. L., Puerari I., Freeman K. C., Groess R., Block E. K., eds., p. 165

Carignan C., 1985a, ApJ, 299, 59

Carignan C., 1985b, ApJS, 58, 107

Carignan C., Beaulieu S., 1989, ApJ, 347, 760

Carignan C., Freeman K. C., 1988, ApJL, 332, L33

Carignan C., Puche D., 1990, AJ, 100, 641

Casertano S., 1983, MNRAS, 203, 735

Chemin L., de Blok W. J. G., Mamon G. A., 2011, AJ, 142, 109

de Blok W. J. G., McGaugh S. S., 1998, ApJ, 508, 132

de Blok W. J. G., McGaugh S. S., Rubin V. C., 2001, AJ, 122, 2396

de Blok W. J. G., Walter F., Brinks E., Trachternach C., Oh S.-H., Kennicutt, Jr. R. C., 2008, AJ, 136, 2648

de Vaucouleurs G., 1956, Survey of bright galaxies south of -35 deg. declination with the 30-inch Reynolds reflector (1952-1955)

de Vaucouleurs G., de Vaucouleurs A., Corwin, Jr. H. G., Buta R. J., Paturel G., Fouqué P., 1991, Third Reference Catalogue of Bright Galaxies. Volume I: Explanations and references. Volume II: Data for galaxies between 0^h and 12^h. Volume III: Data for galaxies between 12^h and 24^h.

Einasto J., 1969, Astronomische Nachrichten, 291, 97

Famaey B., Binney J., 2005, MNRAS, 363, 603

Famaey B., McGaugh S. S., 2012, Living Reviews in Relativity, 15, 10

Freedman W. L., Madore B. F., Gibson B. K. et al., 2001, ApJ, 553, 47

Fukushige T., Makino J., 2001, ApJ, 557, 533

Gentile G., Famaey B., de Blok W. J. G., 2011, A&A, 527, A76+

Gieren W., Pietrzyński G., Soszyński I. et al., 2005, ApJ, 628, 695

Gieren W., Pietrzyński G., Soszyński I. et al., 2008, ApJ, 672, 266

Gieren W., Pietrzyński G., Soszyński I. et al., 2009, ApJ, 700, 1141

Gottesman S. T., 1980, AJ, 85, 824

Höglund B., Roberts M. S., 1965, ApJ, 142, 1366

Hubble E. P., 1926, ApJ, 64, 321

Jobin M., Carignan C., 1990, AJ, 100, 648

Karachentsev I. D., Karachentseva V. E., Huchtmeier W. K., Makarov D. I., 2004, AJ, 127, 2031

Kelson D. D., Illingworth G. D., Tonry J. L. et al., 2000, ApJ, 529, 768

Kennicutt, Jr. R. C., Armus L., Bendo G. et al., 2003, PASP, 115, 928

Kent S. M., 1987, AJ, 93, 816

Kormendy J., Freeman K. C., 2004, in IAU Symposium, Vol. 220, Dark Matter in Galaxies, Ryder S., Pisano D., Walker M., Freeman K., eds., p. 377

Kormendy J., Norman C. A., 1979, ApJ, 233, 539

Lake G., 1989, ApJL, 345, L17

Mamon G. A., Łokas E. L., 2005, MNRAS, 363, 705

Merritt D., Graham A. W., Moore B., Diemand J., Terzić B., 2006, AJ, 132, 2685

Milgrom M., 1983a, ApJ, 270, 371

Milgrom M., 1983b, ApJ, 270, 365

Milgrom M., 1988, ApJ, 333, 689

Milgrom M., 1991, ApJ, 367, 490

Milgrom M., Braun E., 1988, ApJ, 334, 130

Navarro J. F., Frenk C. S., White S. D. M., 1997, ApJ, 490, 493

Navarro J. F., Hayashi E., Power C. et al., 2004, MNRAS, 349, 1039

Oh S.-H., de Blok W. J. G., Walter F., Brinks E., Kennicutt, Jr. R. C., 2008, AJ, 136, 2761

Pietrzyński G., Gieren W., Hamuy M. et al., 2010, AJ, 140, 1475

Pisano D. J., Wilcots E. M., Elmegreen B. G., 1998, AJ, 115, 975

Puche D., Carignan C., 1991, ApJ, 378, 487

Rawson D. M., Macri L. M., Mould J. R. et al., 1997, ApJ, 490, 517

Roberts M. S., Whitehurst R. N., 1975, ApJ, 201, 327

Rogstad D. H., Chu K., Crutcher R. M., 1979, ApJ, 229, 509

Sandage A., 1961, The Hubble atlas of galaxies

Sanders R. H., 1996, ApJ, 473, 117

Sanders R. H., McGaugh S. S., 2002, ARA&A, 40, 263

Sanders R. H., Verheijen M. A. W., 1998, ApJ, 503, 97

Shostak G. S., 1973, A&A, 24, 411

Soszyński I., Gieren W., Pietrzyński G., Bresolin F., Kudritzki R.-P., Storm J., 2006, ApJ, 648, 375

Spano M., Marcelin M., Amram P., Carignan C., Epinat B., Hernandez O., 2008, MNRAS, 383, 297

Swaters R. A., Sanders R. H., McGaugh S. S., 2010, ApJ, 718, 380

Tolstoy E., Saha A., Hoessel J. G., McQuade K., 1995, AJ, 110, 1640

Trachternach C., de Blok W. J. G., Walter F., Brinks E., Kennicutt, Jr. R. C., 2008, AJ, 136, 2720

van der Hulst J. M., Terlouw J. P., Begeman K. G., Zwitser W., Roelfsema P. R., 1992, in Astronomical Society of the Pacific Conference Series, Vol. 25, Astronomical Data Analysis Software and Systems I, Worrall D. M., Biemesderfer C., Barnes J., eds., p. 131

Verheijen M. A. W., 1997, PhD thesis, PhD thesis, Univ. Groningen, The Netherlands , (1997)

Walter F., Brinks E., de Blok W. J. G. et al., 2008, AJ, 136, 2563

Westmeier T., Braun R., Koribalski B. S., 2011, MNRAS, 410, 2217

Zhao H. S., Famaey B., 2006, ApJL, 638, L9

Zwicky F., 1933, Helvetica Physica Acta, 6, 110